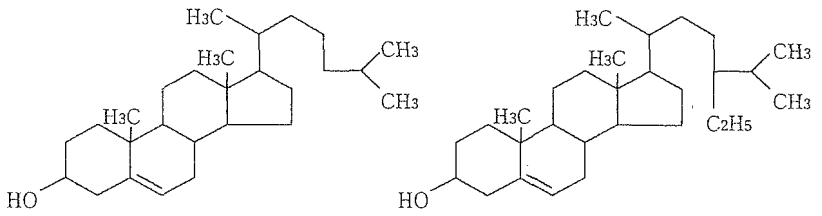

図8　動物性コレステロールと植物性シトステロール

ABCG5とABCG8はそれぞれ6つの膜貫通領域と1つのATP結合ドメインをもち（第Ⅰ章を参照），ヘテロダイマーを形成して機能しているらしい．植物性ステロールの小腸からの吸収を防ぐとともに，胆汁中に排出している．また，マウスにおいてはコレステロールの胆汁中への排出にも関与しているらしい．ABCG5とABCG8の異常は高シトステロール血症をひき起こす．この遺伝性疾患については，興味深いことに，これまでに日本人からは*ABCG5*遺伝子にだけ変異が見つかり，白人からは*ABCG8*遺伝子にだけ変異が見つかっているようである．

ABCG5/G8ヘテロダイマーは小腸上皮の管腔に面した刷子縁膜に発現している．動物にとって必要なコレステロールも必要でない植物や甲殻類のステロールも胆汁酸によって一緒に可溶化されるため，それらは同じように小腸上皮を通過しようとするだろう．その小腸上皮の管腔側でABCG5/G8は体にとって不必要な植物や甲殻類のステロールを排出し，血管側に発現したABCA1が必要なコレステロールを吸収するという協調的な役割分担が予想される．しかし，このような役割分担はあくまで予想であり，このシステムがコレステロールの選別吸収に実際にどのように寄与しているのかは，これから実証する必要がある．

3.7　マクロファージにおけるABCA1の生理的役割

肝臓では，アセチルCoAを出発物質として20段階以上の酵素反応によって毎日約200～250 mgのコレステロールが生合成されている．しかし，それだけでは足らず，毎日食事によって摂取している．マクロファージなどの末梢細胞では，肝臓と同様にコレステロールを合成するが，それと同時に肝臓から低密

度リポ蛋白質（LDL）の形で供給される．肝臓では，コレステロールは胆汁酸に変換され消化管へ放出されるが，マクロファージではコレステロールは異化されない．HDLとして肝臓へ逆転送される経路が，マクロファージからコレステロールが放出される唯一の経路である（図6）．

血中HDLが激減するタンジール病や家族性低HDL症の患者の*ABCA1*遺伝子に多くの変異が同定され，HDLが形成されない原因が，ABCA1の異常であることが明らかになった．それまで，細胞膜からHDL粒子へのコレステロール流出は細胞膜とHDL粒子の間に形成された濃度勾配によって非特異的に行なわれると考えられてきただけに，そこにATP依存トランスポーター型蛋白質であるABCA1が重要な役割を果たしているという発見は衝撃であった．

ABCA1を培養細胞に安定発現させ，脂質の結合していないアポA-Ⅰを培地中に加えると，アポA-Ⅰにコレステロールとリン脂質が結合したHDLが培地中に出現する．アポA-Ⅰは，約240アミノ酸からなる水溶性の蛋白質で，その大部分がαヘリックス構造をとっている．そのαヘリックス構造の片面に疎水性のアミノ酸が並んでおり，リン脂質とコレステロール複合体をアポA-Ⅰが疎水面を内側にしてベルトのように巻きつきリン脂質の疎水性部分を隠すことによって血中に溶かすと考えられている．ABCA1を発現していない細胞にアポA-Ⅰを添加してもHDLはまったく形成されないことから，新生HDL（preβ-HDLと呼ばれる）の形成にはABCA1が必須である．

これまでにタンジール病や家族性低HDL症の患者の*ABCA1*遺伝子に多くの変異が同定されているが，その多くがABCA1の第1細胞外ドメインかATP結合領域にマップされている．第1細胞外ドメインのアミノ酸配列はニワトリからヒトまで非常によく保存されているため，アポA-Ⅰとの相互作用などへの関与も示唆されている．また，ATP結合領域の変異によってHDLが形成されなくなる．他のトランスポーター型のABC蛋白質の研究から，ATP結合領域の変異によってトランスポーターとしての活性がなくなることがわかっている．それらの事実から予想されるABCA1の作用メカニズムは，以下のようなものであろう（図9）．つまり，①アポA-ⅠがABCA1の細胞外ドメインと相互作用する．②ABCA1がATP加水分解することによって構造変化する．③膜中のコレステロールとリン脂質がABCA1によって押し出され，アポA-Ⅰと複合体を形成する．

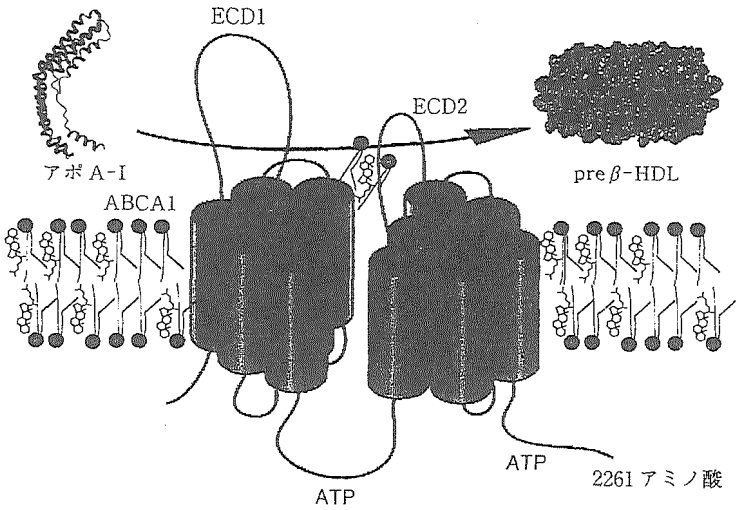

図9　ABCA1 による HDL 形成のモデル

しかし，実際に ABCA1 が ATP のエネルギーを用いて，リン脂質とコレステロールを基質として輸送しているのかどうかは議論が分かれており，preβ-HDL 形成のメカニズムはいまだ混沌としている．そこで筆者らは，ヒト ABCA1 にタンジール病で見つかっているアミノ酸置換を導入し，その影響を調べることによって，ABCA1 の機能を明らかにしようと試みた．

3.8　タンジール病変異の影響

ABCA1 の第 1 細胞外ドメインの後半部分アミノ酸番号 587〜597 には，3 つの変異が集中している．ECD1 中の 3 つの変異 R587W，W590S，Q597R（図 7）の影響を ABCA1 の細胞内局在，コレステロール輸送活性について検討した[37]．

まず，ABCA1 の C 末端に GFP を融合させた ABCA1-GFP に変異を導入し HEK293 細胞に安定発現させた．野生型 ABCA1-GFP は主に細胞膜に発現し，一部細胞内コンパートメント（early endosome と思われる）に存在した（図 10）．変異体のうち，R587W あるいは Q597R 変異をもつ ABCA1-GFP は細胞膜には発現せず，小胞体に局在した．一方，W590S 変異体は，若干細胞内コンパートメントに存在する比率が増えるが，野生型と同様に細胞膜上にも局在するように見えた．第 1 細胞外ドメインに対するポリクローナル抗体を用いて免疫染色を行なった結果，W590S 変異体は，野生型と同様に第 1 細胞外ドメインを細胞外へ突き出した正しいトポロジーで発現していることが明らかになった．

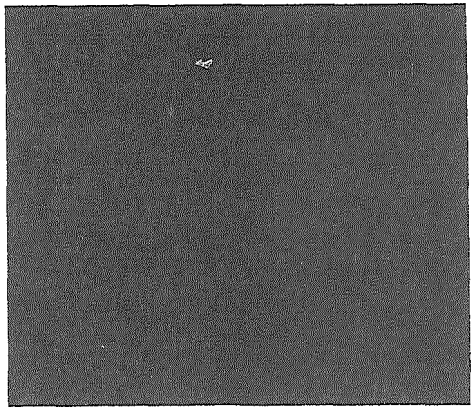

図10　ABCA1 の細胞内局在
GFP と融合させた ABCA1 の発現場所を蛍光顕微鏡で調べた．細胞表面に局在している ABCA1 は細胞外を認識する抗体と反応して，オレンジ色に光っている．

野生型 ABCA1-GFP を発現した細胞ではアポ A-I に依存したリン脂質とコレステロール輸送がはっきり検出される．それ故，C 末端への GFP の融合は ABCA1 の活性には影響を与えない．しかし，R587W，W590S，Q597R の 3 種の変異体を発現した細胞では，アポ A-I に依存したリン脂質とコレステロール輸送がほとんど検出されなかった．以上の結果から，タンジール病患者で見いだされた第 1 細胞外ドメイン上の 3 つの変異のうち，R587W と Q597R は ABCA1 の細胞膜への局在に影響を与えるのに対して，W590S 変異は ABCA1 の活性に影響を与えることが明らかになった．W590S 変異は，ABCA1 の ATP との相互作用にも見かけ上影響を与えなかった[37]．ABCA1 の作用メカニズムを解明する上で，W590S 変異はきわめて興味深い変異体であると思われる．

3.9　ABCA7：自己免疫疾患シェグレン症候群の自己抗原として発見

筆者らは，さらに第 1 細胞外領域の生理的役割を推定するためにホモロジー

検索を行った．その結果，アミノ酸番号270～449の間のアミノ酸配列が自己免疫疾患であるシェグレン症候群の自己抗原SS-Nと高い相同性をもつことを見いだした．さらに自己抗原SS-Nをコードしている遺伝子の全長cDNAを単離した結果，それは*ABCA7*であり，この遺伝子がコードする蛋白質のN末端細胞外ドメインの一部がシェグレン症候群の自己抗原となっていることが明らかになった[36]．ノザン解析を行った結果，ABCA7は胸腺，リンパ節，骨髄，末梢白血球，脾臓，脳などで8～9 kbのpolyA$^+$RNAとして主に発現しており，免疫系の組織および脳で何らかの機能を果たしていることが示唆された[43]．また，組織特異的にスプライシングされていることが明らかになった．ABCA7を培養細胞に安定発現させたところ，ABCA1の場合と同様にアポA-Iに依存してリン脂質とコレステロールを細胞外へ排出することがわかった[43,44]．最近米国のグループは，マウスのABCA7を単離し，細胞に発現させるとリン脂質は排出するが，コレステロールは排出しないと報告した[45]．ABCA7の機能と生理的役割には種特異性があるのかもしれない．

文　献

1) N. Kartner, D. Evernden-Porelle, G. Bradley & V. Ling：*Nature*, 316, 820 (1985).
2) I. B. Roninson, J. E. Chin, K. Choi, P. Gros, D. E. Housman, A. Fojo, D.-w. Shen, M. M. Gottesman & I. Pastan：*Proc. Natl. Acad. Sci. USA*, 83, 4538 (1986).
3) C. Chen, J. E. Chin, K. Ueda, D. P. Clark, I. Pastan, M. M. Gottesman & I. B. Roninson：*Cell*, 47, 381 (1986).
4) K. Ueda, M. M. Cornwell, M. M. Gottesman, I. Pastan, I. B. Roninson, V. Ling & R. J. Riordan：*Biochem. Biophys. Res. Commun.*, 141, 956 (1986).
5) K. Ueda, C. Cardarelli, M. M. Gottesman & I. Pastan：*Proc. Natl. Acad. Sci. USA*, 84, 3004 (1987).
6) A. T. Fojo, K. Ueda, D. J. Slamon, D. G. Poplack, M. M. Gottesman & I. Pastan：*Proc. Natl. Acad. Sci. USA*, 84, 265 (1987)
7) A. M. V. d. Bliek, F. Baas, T. T. H. d. Lange, P. M. Kooiman, T. V. d. Velde-Koerts & P. Borst：*EMBO J.*, 6, 3325 (1987).
8) J. J. M. Smit, A. H. Schinkel, R. P. J. Oude Elferink, A. K. Groen, E. Wagenaar, L. van Deemter, C. A. A. M. Mol, R. Ottenhoff, N. M. T. van der Lugt, M. A. van Roon, M. A. van der Valk, G. J. A. Offerhaus, A. J. M. Berns & P. Borst：*Cell*, 75, 451 (1993).
9) A. v. Helvoort, A. J. Smith, H. Sprong, I. Fritzsche, A. H. Schinkel, P. Borst & G. v. Meer：*Cell*, 87, 507 (1996).
10) K. Kino, Y. Taguchi, K. Yamada, T. Komano & K. Ueda：*FEBS Lett*, 399, 29 (1996).
11) A. J. Smith, A. van Helvoort, G. van Meer, K. Szabo, E. Welker, G. Szakacs, A. Varadi, B. Sarkadi & P. Borst：*J. Biol. Chem.*, 275, 23530 (2000).

12) D. F. Tang-Wai, A. Brossi, L. D. Arnold & P. Gros：*Biochemistry*, 32, 6470 (1993).
13) K. Ueda, N. Okamura, M. Hirai, Y. Tanigawara, T. Saeki, N. Kioka, T. Komano & R. Hori：*J. Biol. Chem.*, 267, 24248 (1992).
14) K. Ueda, Y. Taguchi & M. Morishima："Seminars in Cancer Biology", ed. by Borst, P., Academic Press, UK, p. 151 (1997).
15) Y. Takada, K. Yamada, Y. Taguchi, K. Kino, M. Matsuo, S. J. Tucker, T. Komano, T. Amachi & K. Ueda：*Biochim. Biophys. Acta*, 1373, 131 (1998).
16) K. Nagata, M. Nishitani, M. Matsuo, N. Kioka, T. Amachi & K. Ueda：*J. Biol. Chem.*, 275, 17626 (2000).
17) N. Inagaki, T. Gonoi & S. Seino：*FEBS Lett.*, 409, 232 (1997).
18) Y. Zhou, J. H. Morais-Cabral, A. Kaufman & R. MacKinnon：*Nature*, 414, 43 (2001).
19) K. Tanabe, S. J. Tucker, M. Matsuo, P. Proks, F. M. Ashcroft, S. Seino, T. Amachi & K. Ueda：*J. Biol. Chem.*, 274, 3931 (1999).
20) N. Zerangue, B. Schwappach, Y. Jan & L. Jan：*Neuron*, 22, 537 (1999).
21) K. Ueda, N. Inagaki & S. Seino：*J. Biol. Chem.*, 272, 22983 (1997).
22) M. Matsuo, S. J. Tucker, F. M. Ashcroft, T. Amachi & K. Ueda：*FEBS Lett.*, 458, 292 (1999).
23) M. Matsuo, N. Kioka, T. Amachi & K. Ueda：*J. Biol. Chem.*, 274, 37479 (1999).
24) K. Ueda, J. Komine, M. Matsuo, S. Seino & T. Amachi：*Proc. Natl. Acad. Sci. USA*, 96, 1268 (1999).
25) M. Matsuo, K. Tanabe, N. Kioka, T. Amachi & K. Ueda：*J. Biol. Chem.*, 275, 28757 (2000).
26) T. Matsuoka, K. Matsushita, Y. Katayama, A. Fujita, K. Inageda, M. Tanemoto, A. Inanobe, S. Yamashita, Y. Matsuzawa & Y. Kurachi：*Circ. Res.*, 87, 873 (2000).
27) M. Matsuo, S. Trapp, Y. Tanizawa, N. Kioka, T. Amachi, Y. Oka, F. M. Ashcroft & K. Ueda：*J. Biol. Chem.*, 275, 41184 (2000).
28) A. Brooks-Wilson, M. Marcil, S. Clee, L. Zhang, K. Roomp, M. van Dam, L. Yu, C. Brewer, J. Collins, H. Molhuizen, O. Loubser, B. Ouelette, K. Fichter, K. Ashbourne-Excoffon, C. Sensen, S. Scherer, S. Mott, M. Denis, D. Martindale, J. Frohlich, K. Morgan, B. Koop, S. Pimstone, J. Kastelein & M. Hayden：*Nature Genet.*, 22, 336 (1999).
29) M. Bodzioch, E. Orso, J. Klucken, T. Langmann, A. Bottcher, W. Diederich, W. Drobnik, S. Barlage, C. Buchler, M. Porsch-Ozcurumez, W. Kaminski, H. Hahmann, K. Oette, G. Rothe, C. Aslanidis, K. Lackner & G. Schmitz：*Nature Genet.*, 22, 347 (1999).
30) S. Rust, M. Rosier, H. Funke, J. Real, Z. Amoura, J. Piette, J. Deleuze, H. Brewer, N. Duverger, P. Denefle & G. Assmann：*Nature Genet.*, 22, 352 (1999).
31) S. S. Strautnieks, L. N. Bull, A. S. Knisely, S. A. Kocoshis, N. Dahl, H. Arnell, E. Sokal, K. Dahan, S. Childs, V. Ling, M. S. Tanner, A. F. Kagalwalla, A. Nemeth, J. Pawlowska, A. Baker, G. Mieli-Vergani, N. B. Freimer, R. M. Gardiner & R. J. Thompson：*Nature Genet.*, 20, 233 (1998).
32) D. S. Fredrickson：*J. Clin. Invest.*, 43, 228 (1964).
33) M. J. van Dam, E. de Groot, S. M. Clee, G. K. Hovingh, R. Roelants, A. Brooks-Wilson, A. H. Zwinderman, A. J. Smit, A. H. Smelt, A. K. Groen, M. R. Hayden & J. J. Kastelein：*Lancet*, 359, 37 (2002).
34) T. Langmann, J. Klucken, M. Reil, G. Liebisch, M. Luciani, G. Chimini, W. Kaminski &

G. Schmitz : *Biochem. Biophys. Res. Commun.*, 257, 29 (1999).
35) L.-X. Zhao, C.-J. Zhou, A. Tanaka, M. Nakata, T. Hirabayashi, T. Amachi, S. Shioda, K. Ueda & N. Inagaki : *Biochem. J.*, 350, 865 (2000).
36) A. R. Tanaka, Y. Ikeda, S. Abe-Dohmae, R. Arakawa, K. Sadanami, A. Kidera, S. Nakagawa, T. Nagase, R. Aoki, N. Kioka, T. Amachi, S. Yokoyama & K. Ueda : *Biochem. Biophys. Res. Commun.*, 283, 1019 (2001).
37) A. R. Tanaka, S. Abe-Dohmae, T. Ohnishi, R. Aoki, G. Morinaga, K. I. Okuhira, Y. Ikeda, F. Kano, M. Matsuo, N. Kioka, T. Amachi, M. Murata, S. Yokoyama & K. Ueda : *J. Biol. Chem.*, 278, 8815 (2003).
38) E. Orso, C. Broccardo, W. E. Kaminski, A. Bottcher, G. Liebisch, W. Drobnik, A. Gotz, O. Chambenoit, W. Diederich, T. Langmann, T. Spruss, M.-F. Luciani, G. Rothe, K. J. Lackner, G. Chimini & G. Schmitz : *Nature Genet.*, 24, 192 (2000).
39) H. Allayee, B. A. Laffitte & A. J. Lusis : *Science*, 290, 1709 (2000).
40) T. Ohama, K. Hirano, Z. Zhang, R. Aoki, K. Tsujii, Y. Nakagawa-Toyama, K. Tsukamoto, C. Ikegami, A. Matsuyama, M. Ishigami, N. Sakai, H. Hiraoka, K. Ueda, S. Yamashita & Y. Matsuzawa : *Biochem. Biophys. Res. Commun.*, 296, 625 (2002).
41) A. D. Attie, Y. Hamon, A. R. Brooks-Wilson, M. P. Gray-Keller, M. L. MacDonald, V. Rigot, A. Tebon, L. H. Zhang, J. D. Mulligan, R. R. Singaraja, J. J. Bitgood, M. E. Cook, J. J. Kastelein, G. Chimini & M. R. Hayden : *J. Lipid. Res.*, 43, 1610 (2002).
42) J. D. Mulligan, M. T. Flowers, A. Tebon, J. J. Bitgood, C. Wellington, M. R. Hayden & A. D. Attie : *J. Biol. Chem.*, 278, 13356 (2003).
43) Y. Ikeda, S. Abe-Dohmae, Y. Munehira, R. Aoki, S. Kawamoto, A. Furuya, K. Shitara, T. Amachi, N. Kioka, M. Matsuo, S. Yokoyama & K. Ueda : *Biochem. Biophys. Res. Commun.*, 311, 313 (2003).
44) S. Abe-Dohmae, Y. Ikeda, M. Matsuo, M. Hayashi, K. I. Okuhira, K. Ueda & S. Yokoyama : *J. Biol. Chem.*, 279, 604 (2004).
45) N. Wang, D. Lan, M. Gerbod-Giannone, P. Linsel-Nitschke, A. W. Jehle, W. Chen, L. O. Martinez & A. R. Tall : *J. Biol. Chem.*, 278, 42906 (2003).

V. ABC 蛋白質の立体構造研究——現状と課題

加藤博章，小段篤史，柴田洋之

ABC 蛋白質は，よく似たアミノ酸配列をもっているにもかかわらず，ポンプ，チャンネル，レギュレーターなど，それぞれ特異的な機能を担っている．そこで，それぞれの機能がどのような仕組みで実現しているのかを明らかにするためには，分子構造（立体構造）を原子レベルで明らかにする必要がある．ABC 蛋白質は，ATP の化学エネルギーを動力源として活動する分子機械である．したがって，ATP をいかに駆動力として利用しているのか，その仕組みにも興味がもたれる．筆者らは，ヒト MDR1 の X 線結晶構造解析を目指して，研究を開始した．これまでのところ，立体構造を決定するまでには至っていないものの，昆虫細胞を用いて，非常に大量（1 リットルの培養細胞から数ミリグラム）の発現蛋白質を精製できる系を確立することができている．しかし，この間，原核生物由来の ABC 蛋白質では，ATP 結合サブユニットの立体構造が 11 例決定され（2004 年 4 月現在；表 1.），ATP の加水分解の反応メカニズムや，WalkerA/B モチーフなど ABC 蛋白質に特徴的な配列の役割が構造に基づいて解釈されてきた．そして，2001 年には，大腸菌由来の MDR1 ホモログである，MsbA の全体構造が 4.5 Å 分解能で決定されるに至り[1]，翌年には，大腸菌のビタミン B_{12} の取り込みを行っているインポーターである BtuCD の立体構造が決定された[2]．さらに，2003 年には，*Vibrio cholera* 菌由来の MsbA の立

Available online at www.sciencedirect.com

SCIENCE DIRECT®

Life Sciences 78 (2006) 882 – 887

Life Sciences

www.elsevier.com/locate/lifescie

Vagal stimulation suppresses ischemia-induced myocardial interstitial norepinephrine release

Toru Kawada [a,*], Toji Yamazaki [b], Tsuyoshi Akiyama [b], Meihua Li [a], Hideto Ariumi [a], Hidezo Mori [b], Kenji Sunagawa [c], Masaru Sugimachi [a]

[a] *Department of Cardiovascular Dynamics, Advanced Medical Engineering Center, National Cardiovascular Center Research Institute, 5-7-1 Fujishirodai, Suita, Osaka 565-8565, Japan*

[b] *Department of Cardiac Physiology, National Cardiovascular Center Research Institute, Osaka 565-8565, Japan*

[c] *Department of Cardiovascular Medicine, Graduate School of Medical Sciences, Kyushu University, Fukuoka 812-8582, Japan*

Received 30 November 2004; accepted 31 May 2005

Abstract

Although electrical vagal stimulation exerts beneficial effects on the ischemic heart such as an antiarrhythmic effect, whether it modulates norepinephrine (NE) and acetylcholine (ACh) releases in the ischemic myocardium remains unknown. To clarify the neural modulation in the ischemic region during vagal stimulation, we examined ischemia-induced NE and ACh releases in anesthetized and vagotomized cats. In a control group (VX, $n=8$), occlusion of the left anterior descending coronary artery increased myocardial interstitial NE level from 0.46±0.09 to 83.2±17.6 nM at 30–45 min of ischemia (mean±SE). Vagal stimulation at 5 Hz (VS, $n=8$) decreased heart rate by approximately 80 beats/min during the ischemic period and suppressed the NE release to 24.4±10.6 nM ($P<0.05$ from the VX group). Fixed-rate ventricular pacing (VSP, $n=8$) abolished this vagally mediated suppression of ischemia-induced NE release. The vagal stimulation augmented ischemia-induced ACh release at 0–15 min of ischemia (VX: 11.1±2.1 vs. VS: 20.7±3.9 nM, $P<0.05$). In the VSP group, the ACh release was not augmented. In conclusion, vagal stimulation suppressed the ischemia-induced NE release and augmented the initial increase in the ACh level. These modulations of NE and ACh levels in the ischemic myocardium may contribute to the beneficial effects of vagal stimulation on the heart during acute myocardial ischemia.

Keywords: Acetylcholine; Coronary occlusion; Ventricular pacing

Introduction

Acute myocardial ischemia disrupts normal neural regulation of the heart (Armour, 1999). During prolonged ischemia, myocardial interstitial norepinephrine (NE) and acetylcholine (ACh) levels are increased in the ischemic region via local releasing mechanisms independent of efferent autonomic activities (Schömig et al., 1987; Lameris et al., 2000; Kawada et al., 2000, 2001). The excess NE release is thought to aggravate ischemic injury to the myocardium (Schömig et al., 1987). On the other hand, vagal stimulation exerts antiarrhythmic effects in the early phase of acute myocardial ischemia (Rosenshtraukh et al., 1994; Vanoli et al., 1991). A recent study from our laboratory demonstrated that vagal stimulation improved the survival rate of chronic heart failure after myocardial infarction in rats (Li et al., 2004), suggesting a long-term ameliorative effect of direct neural interventions against certain heart diseases.

With respect to electrical stimulation of the vagus, whether it alters myocardial interstitial NE and ACh levels in the ischemic region during acute myocardial ischemia remains unknown. To test the hypothesis that vagal stimulation increases the ACh level and suppresses the NE level in the ischemic region, we measured myocardial interstitial NE and ACh levels during acute myocardial ischemia in anesthetized cats using a cardiac microdialysis technique (Akiyama et al., 1991, 1994; Yamazaki et al., 1997). Effects of vagal stimulation were examined with or without fixed-rate ventricular pacing.

* Corresponding author. Tel.: +81 6 6833 5012x2427; fax: +81 6 6835 5403.
E-mail address: torukawa@res.ncvc.go.jp (T. Kawada).

0024-3205/$ - see front matter © 2005 Elsevier Inc. All rights reserved.
doi:10.1016/j.lfs.2005.05.087

Materials and methods

This investigation conforms with the *Guide for the Care and Use of Laboratory Animals* published by the US National Institutes of Health (NIH Publication No. 85-23, revised 1996).

Surgical preparation

Twenty-four adult cats weighing from 2.2 to 3.8 kg were anesthetized by an intraperitoneal injection of pentobarbital sodium (30–35 mg/kg) and ventilated mechanically with room air mixed with oxygen. The depth of anesthesia was maintained with a continuous intravenous infusion of pentobarbital sodium (1–2 mg kg^{-1} h^{-1}) through a catheter inserted from the right femoral vein to the inferior vena cava. Systemic arterial pressure (AP) was monitored from a catheter inserted from the right femoral artery into the abdominal aorta. Heart rate (HR) was determined from an electrocardiogram using a cardiotachometer. Esophageal temperature of the animal was measured using a thermometer (CTM-303, TERUMO, Japan) and was maintained at around 37 °C using a heated pad and a lamp.

Bilateral vagal nerves were sectioned through a midline cervical incision. With the animal in the lateral position, the left fifth and sixth ribs were resected to expose the heart. A dialysis probe was implanted, using a fine guiding needle, into the anterolateral free wall of the left ventricle perfused by the left anterior descending coronary artery (LAD). A 3-0 silk suture was passed around the LAD just distal to the first diagonal branch for later coronary occlusion. When an experimental protocol required electrical stimulation of the vagal efferent nerves, bipolar platinum electrodes were attached to the cardiac end of sectioned vagal nerves bilaterally. The nerves and electrodes were covered with warmed mineral oil for insulation. When an experimental protocol required cardiac pacing, bipolar stainless-steel wire electrodes were sutured at the left ventricular apex away from the implanted dialysis probe. Heparin sodium (100 U/kg) was administered intravenously to prevent blood coagulation.

In additional four anesthetized cats, the left ventricle was implanted with a dialysis probe and a pair of pacing electrodes to examine the effects of left ventricular pacing alone on the myocardial interstitial NE levels. The dialysis probe and pacing leads were placed in the same manner as described in the previous paragraph.

At the end of the experiment, the experimental animals were killed with an overdose of pentobarbital sodium. Postmortem examination confirmed that the dialysis probe had been implanted within the left ventricular myocardium.

Dialysis technique

The materials and properties of the dialysis probe have been previously described (Akiyama et al., 1991, 1994). Briefly, we designed a transverse dialysis probe. A dialysis fiber (13 mm length, 310 μm O.D., 200 μm I.D.; PAN-1200, 50,000 molecular weight cutoff, Asahi Chemical, Japan) was glued at both ends to polyethylene tubes (25 cm length, 500 μm O.D., 200 μm I.D.). The dialysis probe was perfused at a rate of 2 μl/min with Ringer solution containing the cholinesterase inhibitor eserine (100 μM). Dialysate sampling was initiated 2 h after implanting the dialysis probe, when the dialysate concentrations of NE and ACh had reached steady states (Akiyama et al., 1991, 1994). The actual dialysate sampling lagged behind a given collection period by 5 min taking into account the dead space volume between the dialysis membrane and the sample tube. Dialysate concentrations of NE and ACh were measured separately by high performance liquid chromatography with electrochemical detection (DTA-300, Eicom, Japan). Details of the NE and ACh measurements have been previously described (Akiyama et al., 1991, 1994).

Protocols

Protocol 1 (VX, n = 8)

As a control experiment, we measured ischemia-induced NE and ACh releases during 60-min LAD occlusion in vagotomized animals. After collecting a 15-min baseline dialysate sample, we occluded the LAD for 60 min and collected four consecutive 15-min dialysate samples during acute myocardial ischemia. We then loosened the LAD snare and collected a 15-min dialysate sample during reperfusion.

Protocol 2 (VS, n = 8)

We examined the effects of vagal stimulation on ischemia-induced NE and ACh releases. To avoid possible preconditioning mimetic effects of ACh released by vagal stimulation (Przyklenk and Kloner, 1995; Kawada et al., 2002a), we initiated the bilateral vagal stimulation (5 Hz, 1 ms in pulse duration and 10 V in pulse amplitude) at the onset of LAD occlusion. The vagal stimulation continued for the 60-min ischemic period and the 15-min reperfusion period.

Protocol 3 (VSP, n = 8)

To eliminate the effects of bradycardia associated with vagal stimulation, we performed vagal stimulation under fixed-rate pacing conditions. We initiated the bilateral vagal stimulation (5 Hz, 1 ms in pulse duration and 10 V in pulse amplitude) and paced the heart from the onset of LAD occlusion to the conclusion of the experimental period. The ventricular pacing rate was set close to the HR recorded immediately before the LAD occlusion.

Supplemental protocol (n = 4)

To examine the effects of left ventricular pacing on the myocardial interstitial NE levels, we collected 15-min dialysate samples under control conditions as well as under left ventricular pacing at 170 beats/min.

Statistical analysis

All data are presented as means ± SE values. In each group, the effects of LAD occlusion on dialysate concentrations of NE and ACh were examined using a repeated-measures analysis of

variance followed by a Dunnett test against respective baseline concentrations. Because the variance of NE data was very large and increased with mean, the NE data were compared after the logarithmic transform (Snedecor and Cochran, 1989). Differences were considered significant at $P<0.05$. To examine the effects of vagal stimulation with or without the ventricular pacing, dialysate concentrations of NE and ACh were compared among the three groups at each corresponding time period using one-way analysis of variance followed by a Student–Newman–Keuls test for all pairwise comparisons (Glantz, 2002). The NE data were compared after the logarithmic transform. Differences were considered significant at $P<0.05$. Heart rate and mean AP were determined immediately before the coronary occlusion (designated as time 0), after 5, 10, 15, 30, 45, and 60 min of the occlusion, and after 15 min of reperfusion. One-way analysis of variance followed by a Student–Newman–Keuls test was also applied to compare HR and mean AP among the three groups at each time point.

Results

Fig. 1 depicts LAD occlusion-induced myocardial interstitial NE accumulation within the ischemic zone. The inset shows the NE levels during baseline conditions in a magnified ordinate. In the VX group, LAD occlusion increased the NE level approximately 200 fold compared to the baseline level at 45–60 min. This occlusion-induced NE accumulation was significantly suppressed in the VS group compared with the VX group in 15–30, 30–45, and 45–60 min time periods. The difference between the VS and VX groups did not reach statistical significance at the reperfusion period. In the VSP group, in which HR was kept constant, vagal stimulation did not attenuate the occlusion-induced NE accumulation. In the supplemental protocol, the baseline myocardial interstitial NE level was 0.17±0.01 nM. The NE level during ventricular pacing at 170 beats/min was 0.21±0.09 nM.

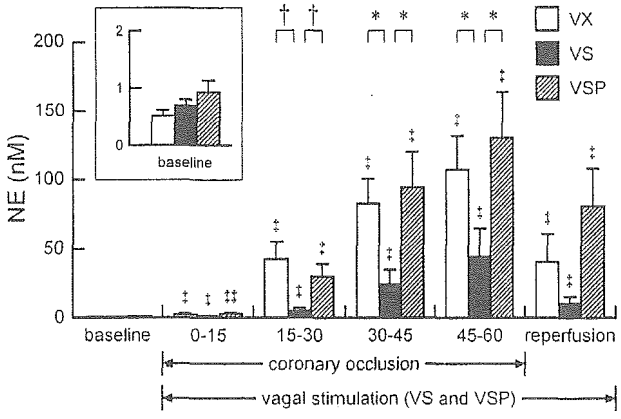

Fig. 1. Coronary occlusion-induced norepinephrine (NE) accumulation in the ischemic myocardium. VX: vagotomy, VS: vagal stimulation, VSP: vagal stimulation with ventricular pacing. The inset shows the baseline conditions with a magnified ordinate. Data are means±SE. $^{\ddagger}P<0.01$ and $^{\ddagger\ddagger}P<0.05$ from the corresponding baseline value in each group. $^{\dagger}P<0.01$ and $^{*}P<0.05$ by all pairwise comparisons among the three groups.

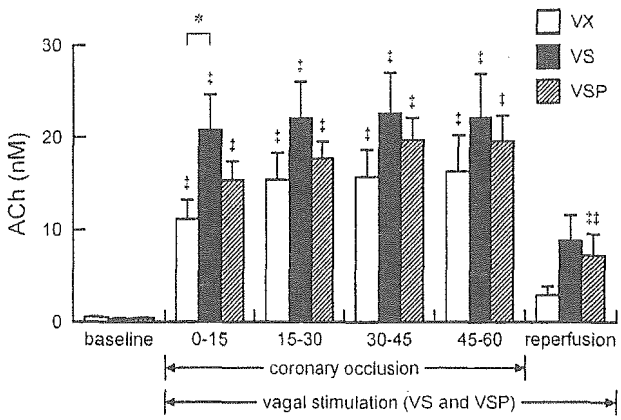

Fig. 2. Coronary occlusion-induced acetylcholine (ACh) accumulation in the ischemic myocardium. Data are means±SE. $^{\ddagger}P<0.01$ and $^{\ddagger\ddagger}P<0.05$ from the corresponding baseline value in each group. $^{*}P<0.05$ by all pairwise comparisons among the three groups.

Fig. 2 shows LAD occlusion-induced myocardial interstitial ACh accumulation within the ischemic zone. In the VX group, LAD occlusion increased the ACh level approximately 20 times higher than the baseline level at 45–60 min. The ACh level at 0–15 min was significantly higher in the VS than the VX group. For the rest of the ischemic period and reperfusion period, the differences between the VS and VX groups were not significant. The ACh levels in the VSP group did not differ from the VX group for any of the sampling periods.

Fig. 3 summarizes changes in HR and mean AP. In the VS group, HR was decreased by approximately 80 beats/min compared with the VX group at 5 min of coronary occlusion. The HR decrease continued for the rest of the ischemic period and reperfusion period. In the VSP group, HR was kept close to the preocclusion level, and it did not differ from the VX group

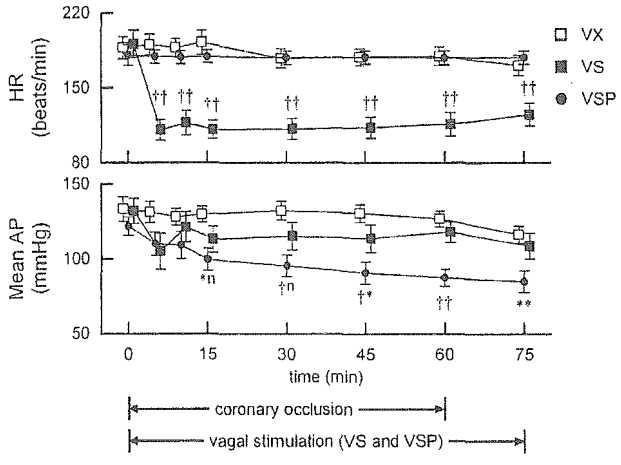

Fig. 3. Time courses of heart rate (HR) and mean arterial pressure (AP) during 60-min ischemia and 15-min reperfusion. The baseline values obtained just before coronary occlusion are plotted at time 0. Data points for VX and VSP groups are slightly displaced along the time axis for better view of overlapping points. Data are means±SE. In the HR data, †† represents statistical significance of $P<0.01$ from both the VX and VSP groups by all pairwise comparisons. In the AP data, when two characters are added to the VSP data point, the first and second characters represent the statistical significance from VX and VS groups, respectively. *, †, and n designate $P<0.05$, $P<0.01$, and "not significant", respectively.

for all the time points. Mean AP did not differ statistically between VX and VS groups. Mean AP in the VSP group progressively decreased and became significantly lower than the VX group after 15 min of the ischemic period. Mean AP in the VSP group was also significantly lower than the VS group after 45 min of the ischemic period.

Discussion

We have shown that electrical vagal stimulation suppressed ischemia-induced NE release and enhanced an initial increase in the ACh levels in the ischemic myocardium. Fixed-rate pacing abolished the suppression of ischemia-induced NE release by vagal stimulation in the present experimental settings.

Effects of vagal stimulation on ischemia-induced NE release

Several mechanisms can be put forward to explain the suppression of ischemia-induced myocardial interstitial NE release by vagal stimulation. First, activation of presynaptic muscarinic receptors on the sympathetic nerve endings inhibits the exocytotic NE release under normal physiological conditions (Levy and Blattberg, 1976). However, the presynaptic inhibition is unlikely the mechanism underlying the vagally mediated suppression of the ischemia-induced NE release because of the following reasons. Although the exocytotic release mechanism participates in the ischemia-induced NE release within the first 20 min of ischemia, the non-exocytotic release mechanism becomes predominant as the ischemic period is prolonged (Akiyama and Yamazaki, 1999). Myocardial ischemia gradually depletes ATP in the ischemic region including sympathetic nerve terminals, which leads to accumulation of axoplasmic NE and reduction of normal Na^+gradient across the plasma membrane in the sympathetic nerve terminals. The NE uptake transporter on the sympathetic nerve terminals, driven by the Na^+gradient, is then reversed, evoking non-exocytotic NE release (Schwartz, 2000). Therefore, the presynaptic inhibition of exocytotic NE release might contribute little to the suppression of ischemia-induced NE release during prolonged ischemia. Furthermore, the presynaptic inhibition of exocytotic NE release becomes less effective during the ischemic insult (Du et al., 1990; Haunstetter et al., 1994). The fact that the ischemia-induced NE release did not differ between the VSP and VX groups is also in opposition to the presynaptic inhibition as a chief mechanism underlying the vagally mediated suppression of ischemia-induced NE release (Fig. 1). Although left ventricular pacing could have affected myocardial interstitial NE levels, the results of the supplemental protocol indicates that changes in the NE levels by ventricular pacing might be negligibly small compared to the ischemia-induced NE release.

Second, the suppression of ischemia-induced NE release by vagal stimulation may be related to myocardial protection via direct vasodiation of the coronary artery. The coronary dilation may enhance collateral flow in the ischemic region and protect against myocardial deterioration evoked by ischemia. Both ACh and vasoactive intestinal polypeptide (VIP) are known to exert direct coronary dilation (Feliciano and Henning, 1998; Gross et al., 1981; Henning and Sawmiller, 2001). VIP is colocalized with ACh in the postganglionic vagal fibers and is released by high-frequency (20 Hz) vagal stimulation. VIP may interact with NE transport or exocytosis like nociceptin (Yamazaki et al., 2001). However, fixed-rate pacing abolished the ability of vagal stimulation to suppress the ischemia-induced NE release. Hence the direct coronary vasodilation and/or interaction with the sympathetic system via VIP might have played little role in suppressing ischemia-induced NE release in the present experimental settings. Another factor that should be taken into account is that the relatively low-frequency (5 Hz) stimulation might have limited the amount of VIP release from the vagal nerve endings.

Third, HR is one of the most important determinants of myocardial oxygen consumption (Mohrman and Heller, 1997). In the present study, HR in the VS group decreased to approximately 60% that of the VX group during the ischemic period (Fig. 3), which slowed the energy consumption of the myocardium. Bradycardia might also decrease ventricular contractility via a force-frequency mechanism (Maughan et al., 1985). In addition, bradycardia may increase coronary perfusion via prolongation of diastolic interval (Buck et al., 1981). These factors slowed energy consumption in the ischemic region including sympathetic nerve terminals, delaying the time course for non-exocytotic NE release. The prevention of excess NE would further reduce myocardial oxygen consumption and decelerate the progression of ischemic injury (Suga et al., 1983). The ischemia-induced NE release did not differ between the VSP and VX groups despite the lower mean AP in the VSP compared with the VX group. Although lowering AP might decrease afterload of the ventricle and reduce energy consumption, the beneficial effect of afterload reduction might have been masked in the VSP group due to inefficient cardiac pumping function associated with asynchrony between sinus rate and ventricular rate. Proper atrioventricular conduction time contributes to the ventricular filling (Meisner et al., 1985). In the VSP group, the sinus rate was reduced by vagal stimulation whereas the ventricular rate was maintained by fixed-rate pacing. Dissociation of the sinus rate and ventricular rate might have impaired the ventricular filling to a variable extent, resulting in a progressive reduction in AP.

Finally, the vagal stimulation decreases ventricular contractile force against sympathetic activation via the direct projections to the ventricle (Nakayama et al., 2001). This mechanism might have also contributed to the reduction of the myocardial oxygen consumption and slowed the progression of ischemic injury in the VS group. However, the ventricular pacing canceled the protective effects in the VSP group, possibly by the adverse influences discussed in the previous paragraph. Further studies are required to isolate the factor(s) most important for the suppression of ischemia-induced NE release by the vagal stimulation.

Effects of vagal stimulation on ischemia-induced ACh release

In contrast to the suppressive effect of NE release, vagal nerve stimulation can exert two opposing influences on ACh release in the ischemic myocardium. The nerve stimulation itself induces exocytotic ACh release from nerve endings. Acute myocardial ischemia impairs conduction of the nerves traversing in the ischemic region (Barber et al., 1983; Inoue and Zipes, 1988; Martins et al., 1989). Acute myocardial ischemia also impairs the exocytotic ACh release in the postischemic myocardium (Kawada et al., 2002b). On the other hand, acute myocardial ischemia causes myocardial ACh release in the ischemic region via a local release mechanism independent of efferent nerve activity (Kawada et al., 2000). Hence, the amount of ACh release was net effects of ACh release evoked by nerve stimulation and ischemia; vagally mediated protection against ischemic injury should augment the former and attenuate the latter.

Although vagal stimulation augmented myocardial interstitial ACh release during the 0–15 min period of coronary occlusion in the VS group than in the VX group, the initial enhancement was not observed in the VSP group. One possible mechanism for the difference in the initial ACh release between the VS and VSP groups is that the progression of ischemia in the VSP group relative to the VS group impaired the vagal nerve conduction in the ischemic region, reducing the exocytotic ACh release. The other possible mechanism is that the high levels of NE might have attenuated the stimulation-induced ACh release from the vagal nerve endings via α-adrenergic mechanisms (Akiyama and Yamazaki, 2000).

There are several limitations to the present study. First, we avoided large myocardial ischemia by occluding LAD just distal to the first diagonal branch. Accordingly, the incidence of lethal ventricular arrhythmia was too low to draw any conclusion as to the effects of vagal stimulation on the arrhythmogenesis. Further studies with larger myocardial ischemia are clearly required to examine the effects of vagal stimulation on the incidence of lethal ventricular arrhythmia in relation to the observed NE and/or ACh levels in the ischemic myocardium. Second, plasma catecolamine levels might have been increased during the LAD occlusion, which might affect HR and cardiac function in the non-ischemic region. Although changes in plasma catecholamine levels may play significant roles in determining systemic hemodynamics, the ischemic region was only poorly perfused. Accordingly, direct effects of plasma catecholamines on the myocardial interstitial NE and ACh levels in the ischemic region might have been limited in the present study.

Conclusion

Electrical vagal stimulation suppressed ischemia-induced NE release in the ischemic myocardium in anesthetized cats. The vagal stimulation augmented ischemia-induced ACh release at the 0–15 min period of ischemia. Although acute myocardial ischemia causes myocardial NE and ACh releases independent of efferent nerve activity, the vagal stimulation was able to modulate both NE and ACh levels in the ischemic region. The suppression of NE release and augmentation of initial ACh release in the ischemic myocardium by vagal stimulation may reduce the ischemic injury to the heart. The direct neural intervention could be a new modality of medical engineering to cope with ischemic heart diseases.

Acknowledgments

This study was supported by Health and Labour Sciences Research Grant for Research on Advanced Medical Technology (H14-Nano-002) from the Ministry of Health Labour and Welfare of Japan, by Grant-in-Aid for Scientific Research (C-15590786) from the Ministry of Education, Science, Sports and Culture of Japan, and by the Program for Promotion of Fundamental Studies in Health Science from the Organization for Pharmaceutical Safety and Research.

References

Akiyama, T., Yamazaki, T., 1999. Norepinephrine release from cardiac sympathetic nerve endings in the in vivo ischemic region. Journal of Cardiovascular Pharmacology 34, S11–S14.

Akiyama, T., Yamazaki, T., 2000. Adrenergic inhibition of endogenous acetylcholine release on postganglionic cardiac vagal nerve terminals. Cardiovascular Research 46, 531–538.

Akiyama, T., Yamazaki, T., Ninomiya, I., 1991. In vivo monitoring of myocardial interstitial norepinephrine by dialysis technique. American Journal of Physiology. Heart and Circulatory Physiology 261, H1643–H1647.

Akiyama, T., Yamazaki, T., Ninomiya, I., 1994. In vivo detection of endogenous acetylcholine release in cat ventricles. American Journal of Physiology. Heart and Circulatory Physiology 266, H854–H860.

Armour, J.A., 1999. Myocardial ischaemia and the cardiac nervous system. Cardiovascular Research 41, 41–54.

Barber, M.J., Mueller, T.M., Henry, D.P., Felten, S.Y., Zipes, D.P., 1983. Transmural myocardial infarction in the dog produces sympathectomy in noninfarcted myocardium. Circulation 67, 787–796.

Buck, J.D., Warltier, D.C., Hardman, H.F., Gross, G.J., 1981. Effects of sotalol and vagal stimulation on ischemic myocardial blood flow distribution in the canine heart. Journal of Pharmacological and Experimental Therapeutics 216, 347–351.

Du, X.J., Dart, A.M., Riemersma, R.A., Oliver, M.F., 1990. Failure of the cholinergic modulation of norepinephrine release during acute myocardial ischemia in the rat. Circulation Research 66, 950–956.

Feliciano, L., Henning, R.J., 1998. Vagal nerve stimulation releases vasoactive intestinal peptide which significantly increases coronary artery blood flow. Cardiovascular Research 40, 45–55.

Glantz, S.A., 2002. Primer of Biostatistics, 5th ed. McGraw-Hill, New York.

Gross, G.J., Buck, J.D., Warltier, D.C., 1981. Transmural distribution of blood flow during activation of coronary muscarinic receptors. American Journal of Physiology. Heart and Circulatory Physiology 240, H941–H946.

Haunstetter, A., Haass, M., Yi, X., Krüger, C., Kübler, W., 1994. Muscarinic inhibition of cardiac norepinephrine and neuropeptide Y release during ischemia and reperfusion. American Journal of Physiology. Regulatory, Integrative and Comparative Physiology 267, R1552–R1558.

Henning, R.J., Sawmiller, D.R., 2001. Vasoactive intestinal peptide: cardiovascular effects. Cardiovascular Research 49, 27–37.

Inoue, H., Zipes, D.P., 1988. Time course of denervation of efferent sympathetic and vagal nerves after occlusion of the coronary artery in the canine heart. Circulation Research 62, 1111–1120.

Kawada, T., Yamazaki, T., Akiyama, T., Sato, T., Shishido, T., Inagaki, M., Takaki, H., Sugimachi, M., Sunagawa, K., 2000. Differential acetylcholine release mechanisms in the ischemic and non-ischemic myocardium. Journal of Molecular and Cellular Cardiology 32, 405–414.

Kawada, T., Yamazaki, T., Akiyama, T., Inagaki, M., Shishido, T., Zheng, C., Yanagiya, Y., Sugimachi, M., Sunagawa, K., 2001. Vagosympathetic interactions in ischemia-induced myocardial norepinephrine and acetylcholine release. American Journal of Physiology. Heart and Circulatory Physiology 280, H216–H221.

Kawada, T., Yamazaki, T., Akiyama, T., Mori, H., Inagaki, M., Shishido, T., Takaki, H., Sugimachi, M., Sunagawa, K., 2002. Effects of brief ischaemia on myocardial acetylcholine and noradrenaline levels in anaesthetized cats. Autonomic Neuroscience 95, 37–42.

Kawada, T., Yamazaki, T., Akiyama, T., Mori, H., Uemura, K., Miyamoto, T., Sugimachi, M., Sunagawa, K., 2002. Disruption of vagal efferent axon and nerve terminal function in the postischemic myocardium. American Journal of Physiology. Heart and Circulatory Physiology 283, H2687–H2691.

Lameris, T.W., de Zeeuw, Sandra, Alberts, G., Boomsma, F., Duncker, D.J., Verdouw, P.D., Veld, A.J., van den Meiracker, A.H., 2000. Time course and mechanism of myocardial catecholamine release during transient ischemia in vivo. Circulation 101, 2645–2650.

Levy, M.N., Blattberg, B., 1976. Effect of vagal stimulation on the overflow of norepinephrine into the coronary sinus during cardiac sympathetic nerve stimulation in the dog. Circulation Research 38, 81–84.

Li, M., Zheng, C., Sato, T., Kawada, T., Sugimachi, M., Sunagawa, K., 2004. Vagal nerve stimulation markedly improves long-term survival after chronic heart failure in rats. Circulation 109, 120–124.

Martins, J.B., Lewis, R., Wendt, D., Lund, D.D., Schmid, P.G., 1989. Subendocardial infarction produces epicardial parasympathetic denervation in canine left ventricle. American Journal of Physiology. Heart and Circulatory Physiology 256, H859–H866.

Maughan, W.L., Sunagawa, K., Burkhoff, D., Graves, W.L. Jr., Hunter, W.C., Sagawa, K., 1985. Effect of heart rate on the canine end-systolic pressure–volume relationship. Circulation 72, 654–659.

Meisner, J.S., McQueen, D.M., Ishida, Y., Vetter, H.O., Bortolotti, U., Strom, J.A., Frater, R.W.M., Peskin, C.S., Yellin, E.L., 1985. Effects of timing of atrial systole on LV filling and mitral valve closure: computer and dog studies. American Journal of Physiology. Heart and Circulatory Physiology 249, H604–H619.

Mohrman, D.E., Heller, L.J., 1997. Cardiovascular Physiology, 4th ed. McGraw-Hill, New York, pp. 47–69.

Nakayama, Y., Miyano, H., Shishido, T., Inagaki, M., Kawada, T., Sugimachi, M., Sunagawa, K., 2001. Heart rate-independent vagal effect on end-systolic elastance of the canine left ventricule under various levels of sympathetic tone. Circulation 104, 2277–2279.

Przyklenk, K., Kloner, R.A., 1995. Low-dose i.v. acetylcholine acts as a "preconditioning-mimetic" in the canine model. Journal of Cardiac Surgery 10, 389–395.

Rosenshtraukh, L., Danilo Jr., P., Anyukhovsky, E.P., Steinberg, S.F., Rybin, V., Brittain-Valenti, K., Molina-Viamonte, V., Rosen, M.R., 1994. Mechanisms for vagal modulation of ventricular repolarization and of coronary occlusion-induced lethal arrhythmias in cats. Circulation Research 75, 722–732.

Schömig, A., Fischer, S., Kurz, T., Richardt, G., Schömig, E., 1987. Nonexocytotic release of endogenous noradrenaline in the ischemic and anoxic rat heart: mechanism and metabolic requirements. Circulation Research 60, 194–205.

Schwartz, J.H., 2000. Neurotransmitters. In: Kandel, E.R., Schwartz, J.H., Jessell, T.M. (Eds.), Principles of Neural Science, 4th ed. McGraw-Hill, New York, pp. 280–297.

Snedecor, G.W., Cochran, W.G., 1989. Statistical Methods, 8th ed. Iowa State, Iowa, pp. 290–291.

Suga, H., Hisano, R., Goto, Y., Yamada, O., Igarashi, Y., 1983. Effect of positive inotropic agents on the relation between oxygen consumption and systolic pressure volume area in canine left ventricle. Circulation Research 53, 306–318.

Vanoli, E., De Ferrari, G.M., Stramba-Badiale, M., Hull Jr., S.S., Foreman, R.D., Schwartz, P.J., 1991. Vagal stimulation and prevention of sudden death in conscious dogs with a healed myocardial infarction. Circulation Research 68, 1471–1481.

Yamazaki, T., Akiyama, T., Kitagawa, H., Takauchi, Y., Kawada, T., Sunagawa, K., 1997. A new, concise dialysis approach to assessment of cardiac sympathetic nerve terminal abnormalities. American Journal of Physiology. Heart and Circulatory Physiology 272, H1182–H1187.

Yamazaki, T., Akiyama, T., Mori, H., 2001. Effects of nociceptin on cardiac norepinephrine and acetylcholine release evoked by ouabain. Brain Research 904, 153–156.

Am J Physiol Heart Circ Physiol 289: H2641–H2648, 2005.
First published July 29, 2005; doi:10.1152/ajpheart.00642.2005.

Dynamic and static baroreflex control of muscle sympathetic nerve activity (SNA) parallels that of renal and cardiac SNA during physiological change in pressure

Atsunori Kamiya,[1] Toru Kawada,[1] Kenta Yamamoto,[1] Daisaku Michikami,[1] Hideto Ariumi,[1] Tadayoshi Miyamoto,[1] Shuji Shimizu,[1] Kazunori Uemura,[1] Takeshi Aiba,[1] Kenji Sunagawa,[2] and Masaru Sugimachi[1]

[1]*Department of Cardiovascular Dynamics, National Cardiovascular Center Research Institute, Osaka; and*
[2]*Department of Cardiovascular Medicine, Kyusyu University Graduate School of Medical Sciences, Fukuoka, Japan*

Submitted 14 June 2005; accepted in final form 26 July 2005

Kamiya, Atsunori, Toru Kawada, Kenta Yamamoto, Daisaku Michikami, Hideto Ariumi, Tadayoshi Miyamoto, Shuji Shimizu, Kazunori Uemura, Takeshi Aiba, Kenji Sunagawa, and Masaru Sugimachi. Dynamic and static baroreflex control of muscle sympathetic nerve activity (SNA) parallels that of renal and cardiac SNA during physiological change in pressure. *Am J Physiol Heart Circ Physiol* 289: H2641–H2648, 2005. First published July 29, 2005; doi:10.1152/ajpheart.00642.2005.—Despite accumulated knowledge on human baroreflex control of muscle sympathetic nerve activity (SNA), whether baroreflex control of muscle SNA parallels that of other SNAs, in particular renal and cardiac SNAs, remains unclear. Using urethane and α-chloralose-anesthetized, vagotomized and aortic-denervated rabbits ($n = 10$), we recorded muscle SNA from tibial nerve by microneurography, simultaneously with renal and cardiac SNAs by wire electrode. To produce a baroreflex open-loop condition, we isolated the carotid sinuses from systemic circulation and altered the intracarotid sinus pressure (CSP) according to a binary white noise sequence of operating pressure ± 20 mmHg (for investigating dynamic characteristics of baroreflex) or in stepwise 20-mmHg increments from 40 to 160 mmHg (for investigating static characteristics of baroreflex). Dynamic high-pass characteristics of baroreflex control of muscle SNA, assessed by the increasing slope of transfer gain, showed that more rapid change of arterial pressure resulted in greater response of muscle SNA to pressure change and that these characteristics were similar to cardiac SNA but greater than renal SNA. However, numerical simulation based on the transfer function shows that the differences in dynamic baroreflex control at various organs result in detectable differences among SNAs only when CSP changes at unphysiologically high rates (i.e., 5 mmHg/s). On the other hand, static reverse-sigmoid characteristics of baroreflex control of muscle SNA agreed well with those of renal or cardiac SNAs. In conclusion, dynamic-linear and static-nonlinear baroreflex control of muscle SNA is similar to that of renal and cardiac SNAs under physiological pressure change.

carotid sinus pressure

ARTERIAL BAROREFLEX CONTROL of efferent sympathetic nerve activity (SNA) has a very important role in circulatory control (3, 23). It powerfully regulates arterial pressure and attenuates physiological perturbations in arterial pressure via the baroreflex feedback-loop system. Without the baroreflex control of SNA, the simple act of standing causes a great fall in arterial pressure, leading to hypoperfusion to the brain and sometimes loss of consciousness (3, 23). In addition, impaired baroreflex control of SNA may be associated with the pathophysiology of cardiovascular diseases (7, 8, 28). Accordingly, baroreflex control of SNA has been an important target in the studies of cardiovascular physiology and pathophysiology. In earlier studies addressing the baroreflex control of SNA in humans, SNA innervating vessels in skeletal muscles, termed muscle SNA, has been directly measured by microneurographic technique (16, 26, 29), and considered as a proxy of systemic SNA. These studies have contributed significantly to the understanding of the baroreflex control of SNA in circulatory physiology (5, 22, 24) [such as during exercise (4, 12, 25), hypoxia (9, 10), orthostasis (2), heating (13), and aging (17, 26, 27)] and pathophysiology [such as hypertension (7, 28), heart failure (8), myocardial infarction (6), obstructive sleep apnea (21), and neurally mediated syncope (19)].

Despite accumulated knowledge on baroreflex control of muscle SNA, whether the control of muscle SNA parallels that of other visceral organs innervated by the sympathetic nerve system, including the kidney and heart, remains unclear. This is because the human microneurographic technique is mainly limited to the upper and lower limbs (16, 18). Although earlier human studies reported that microneurographical muscle SNA correlated with norepinephrine spillovers in the kidney and heart at rest (30, 31), these studies did not assess baroreflex control of SNA. Because of a lack of definitive evidence, the impact of investigating baroreflex control of muscle SNA could be somewhat limited. Accordingly, we tested whether dynamic and static baroreflex control of muscle SNA is similar to that of renal and cardiac SNAs. We recorded muscle SNA by microneurography simultaneously with renal and cardiac SNAs in anesthetized rabbits. We then compared the dynamic-linear and static-nonlinear characteristics of baroreflex control for the three forms of SNAs.

MATERIALS AND METHODS

Preparation. Animals were cared for in strict accordance with the "Guiding Principles for the Care and Use of Animals in the Field of Physiological Science" approved by the Physiological Society of Japan. The experimental protocol was approved by the animal experiment committee of Japan Aerospace Exploration Agency. Ten Japanese white rabbits weighing 2.4–3.3 kg were initially anesthetized by intravenous injection (2 ml/kg) of a mixture of urethane (250 mg/ml) and α-chloralose (40 mg/ml). Anesthesia was maintained by continuously infusing the anesthetics at a rate of 0.33 $ml \cdot kg^{-1} \cdot h^{-1}$ using a syringe pump (CFV-3200, Nihon Kohden, Tokyo). The rabbits were

Address for reprint requests and other correspondence: A. Kamiya, Dept. of Cardiovascular Dynamics, National Cardiovascular Center Research Institute, 5-7-1 Fujishirodai, Suita, Osaka 565-8565, Japan (e-mail: kamiya@ri.ncvc.go.jp).

The costs of publication of this article were defrayed in part by the payment of page charges. The article must therefore be hereby marked "*advertisement*" in accordance with 18 U.S.C. Section 1734 solely to indicate this fact.

mechanically ventilated with oxygen-enriched room air. Bilateral carotid sinuses were isolated vascularly from the systemic circulation by ligating the internal and external carotid arteries and other small branches originating from the carotid sinus regions. The isolated carotid sinuses were filled with warmed physiological saline pre-equilibrated with atmospheric air through catheters inserted via the common carotid arteries. The intracarotid sinus pressure (CSP) was controlled by a servo-controlled piston pump (model ET-126A, Labworks; Costa Mesa, CA). Bilateral vagal and aortic depressor nerves were sectioned in the middle of the neck region to eliminate reflexes from the cardiopulmonary region and the aortic arch. The systemic arterial pressure (AP) was measured using a high-fidelity pressure transducer (Millar Instruments; Houston, TX) inserted retrogradely from the right common carotid artery below the isolated carotid sinus region. Body temperature was maintained at ~38°C with a heating pad.

The left renal sympathetic nerve was exposed retroperitoneally, and the left cardiac sympathetic nerve was exposed through a middle thoracotomy. A pair of stainless steel wire electrodes (Bioflex wire AS633, Cooner Wire) was attached to each of these nerves to record renal and cardiac SNAs. The left tibial nerve was exposed at the right popliteal fossa through incising the flexors in the dorsal middle region of the thigh. A tungsten microelectrode (model 26-05-1, Frederick Haer; Bowdoinham, ME) was inserted into the right tibial nerve to record muscle SNA, based on human (16, 26) and animal (20) microneurography. We identified muscle SNA by the following discharge characteristics: *1*) afferent activity induced by tapping of the calf muscles but not by gently touching the skin, and 2) excitatory and inhibitory responses induced by decreasing and increasing CSP, respectively.

The nerve fibers peripheral to electrodes were ligated securely and crushed to eliminate afferent signals. The nerve and electrodes were covered with a mixture of silicone gel (Silicon Low Viscosity, KWIK-SIL, World Precision Instrument) to insulate and immobilize the electrodes. The preamplified SNA signals were band-pass filtered at 150–1,000 Hz. These nerve signals were full-wave rectified and low-pass filtered with a cutoff frequency of 30 Hz to quantify the nerve activity.

Evaluation of baroreflex control of SNA: dynamic-linear and static nonlinear characteristics. Baroreflex controls of cardiac and renal SNAs have dynamic-linear high-pass and static-nonlinear reverse-sigmoidal characteristics (14). The dynamic high-pass characteristics indicate that more rapid change of arterial pressure is associated with greater SNA response. Identifying the transfer function from baroreceptor pressure input to SNA is the most powerful tool to quantify dynamic-linear characteristics. Importantly, the transfer function can predict linear SNA responses to any baroreceptor pressure input. On the other hand, the baroreflex control also has static-nonlinear reverse-sigmoidal characteristics that cannot be explained by dynamic-linear characteristics, particularly under steady-state condition (14). Accordingly, we evaluated baroreflex control of SNA by assessing both dynamic-linear and static-nonlinear characteristics while opening the baroreflex feedback loop independently for muscle, cardiac, and renal SNAs.

Protocols. After the surgical preparation, the rabbit was maintained supine. *Protocols 1* and *2* described below were conducted to assess static-nonlinear and dynamic-linear characteristics, respectively, in randomized order with an interval of at least 5 min. Both protocols were conducted in all animals (n = 10). In both protocols, bilateral CSP was controlled by a servo-controlled piston pump (14).

In *protocol 1*, CSP was increased stepwise from 40 to 160 mmHg in increments of 20 mmHg. Each pressure step was maintained for 60 s. The three SNAs, CSP, and AP were recorded for 7 min at a sampling rate of 200 Hz using a 12-bit analog-to-digital converter. Data were stored on the hard disk of a dedicated laboratory computer system.

In *protocol 2*, CSP was first matched with systemic AP to obtain the operating AP under the baroreflex closed-loop condition. After at least 5 min of stabilization, the three SNAs, CSP, and AP were recorded for 10 min and stored as in *protocol 1*. The average AP over 10 min was defined as the operating AP. Then, after at least 5 min of stabilization, CSP was randomly assigned at 20 mmHg above or below the operating AP every 500 ms according to a binary white noise sequence in which the input power spectrum of CSP was reasonably flat up to 1 Hz (14). The three SNAs, CSP, and AP were recorded for 10 min and stored for analysis.

Data analysis. SNA signals were normalized by the following steps. First, for each type of SNA, 0 arbitrary unit (au) was assigned to the postmortem noise level. Second, SNA signals were averaged for the last 10 s at CSP level of 40 mmHg in *protocol 1*; 100 au were then assigned to the average SNA. Last, the other SNA signals in both *protocols 1* and *2* were then normalized to these values.

In *protocol 1*, muscle, renal and cardiac SNAs were averaged for the last 10 s of each CSP level. The static-nonlinear relation between CSP and each SNA was parameterized using a four-parameter logistic equation model as follows:

$$\mathrm{SNA} = P_4 + \frac{P_1}{1 + \exp[P_2(\mathrm{CSP} - P_3)]} \quad (1)$$

where P_1 is the response range of SNA (i.e., the difference between the maximum and minimum SNA), P_2 is the coefficient of gain, P_3 is the midpoint CSP of the logistic function, and P_4 is the minimum SNA. We calculated the instantaneous gain from the first derivative of the logistic function, and the maximum gain from $-P_1P_2/4$ at $x = P_3$.

In *protocol 2*, we calculated the transfer (the gain and phase) and coherence functions from CSP input to each SNA. We resampled CSP and SNA at 10 Hz and segmented them into 10 sets of 50% overlapping bins of 2^{10} data points each. The segment length was 102.4 s. which yielded the lowest frequency bound of 0.01 (0.0097) Hz. We subtracted a linear trend and applied a Hanning window for each segment. We then performed fast Fourier transform to obtain frequency spectra of CSP and SNA. We ensemble-averaged the CSP power [$Sxx(f)$], SNA power [$Syy(f)$], and cross power between CSP and SNA [$Syx(f)$] over the 10 segments. Thereafter, we calculated the transfer function [$H(f)$] from CSP to SNA as follows

$$H(f) = \frac{Syx(f)}{Sxx(f)} \quad (2)$$

To quantify the linear dependence between CSP and SNA in the frequency domain, we calculated the magnitude-squared coherence function [Coh(f)] as follows

$$\mathrm{Coh}(f) = \frac{|Syx(f)|^2}{Sxx(f)Syy(f)} \quad (3)$$

The coherence value ranges from zero to unity. Unity coherence indicates a perfect linear dependence between CSP and SNA, whereas zero coherence indicates total independence of these two signals.

Statistical analysis. All data are presented as means ± SD. We used a repeated-measures analysis of variance with post hoc multiple comparisons to compare variables among muscle, renal, and cardiac SNAs. Differences were considered significant when $P < 0.05$.

RESULTS

Static baroreflex characteristics (protocol 1). Muscle SNA decreased in response to stepwise increase in CSP in *protocol 1*. The change in muscle SNA appeared similar to that in renal or cardiac SNA (Fig. 1). The relation between CSP and muscle SNA was fitted to four-parameter logistic function in individual animals. The fitted logistic function of muscle SNA almost superimposed that of renal or cardiac SNA (Fig. 2). The

parameters of P_1, P_2, P_3, and P_4 and the maximal gain (at the midpoint of the sigmoid curve) of muscle SNA were similar to those of renal or cardiac SNA (Fig. 2, Table 1).

Dynamic baroreflex characteristics (protocol 2). In *protocol 2*, the CSP was perturbed according to a binary white noise sequence at 500-ms intervals (Fig. 3). When CSP was increased, muscle SNA decreased, and vice versa. Although the shape of each burst of muscle SNA differed from that of renal or cardiac SNA, the global characteristics of dynamic changes of muscle SNA appeared roughly the same as those of renal and cardiac SNAs.

In a frequency domain analysis (Fig. 4*A*), the gain of the transfer function from CSP to muscle SNA increased as the frequency of CSP perturbation increased between 0.01 and 0.8 Hz, indicating dynamic high-pass characteristics. The transfer gains in renal and cardiac SNAs also showed high-pass characteristics. The increasing slope of the gain between 0.01 and 0.8 Hz for muscle SNA was similar to that for cardiac SNA but steeper than that for renal SNA (Fig. 4*A*, Table 2). The gains between 0.3 and 1 Hz of muscle SNA were similar to those of cardiac SNA but greater than those of renal SNA ($P < 0.05$) (Table 2).

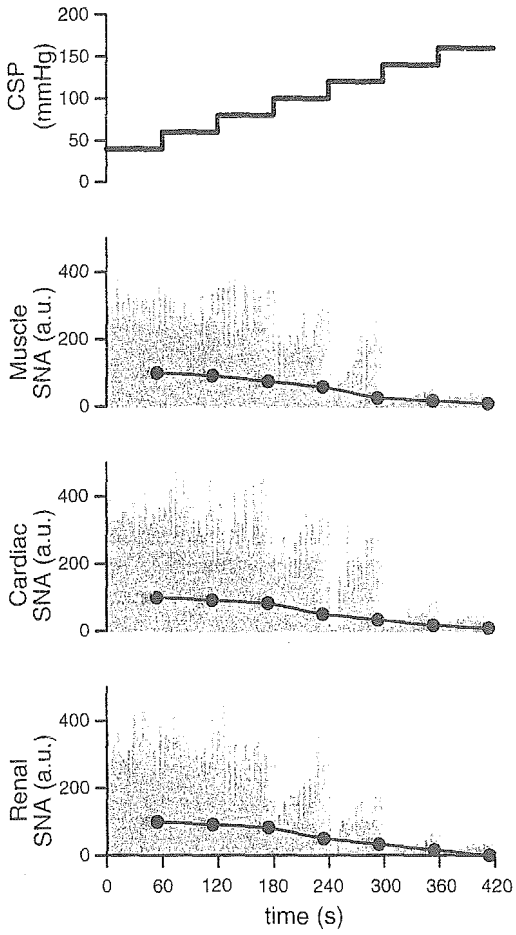

Fig. 1. Representative data of one rabbit in *protocol 1*, showing integrated signals of muscle, cardiac, and renal sympathetic nerve activity (SNA) during stepwise increase in carotid sinus pressure (CSP). Each step is 60 s. Fine lines indicate SNA signals resampled at 10 Hz. Bold lines and closed circles indicate SNA signals averaged over the last 10 s of each CSP level, which were used to determine the static nonlinear characteristics of baroreflex control of each SNA. au, Arbitrary unit.

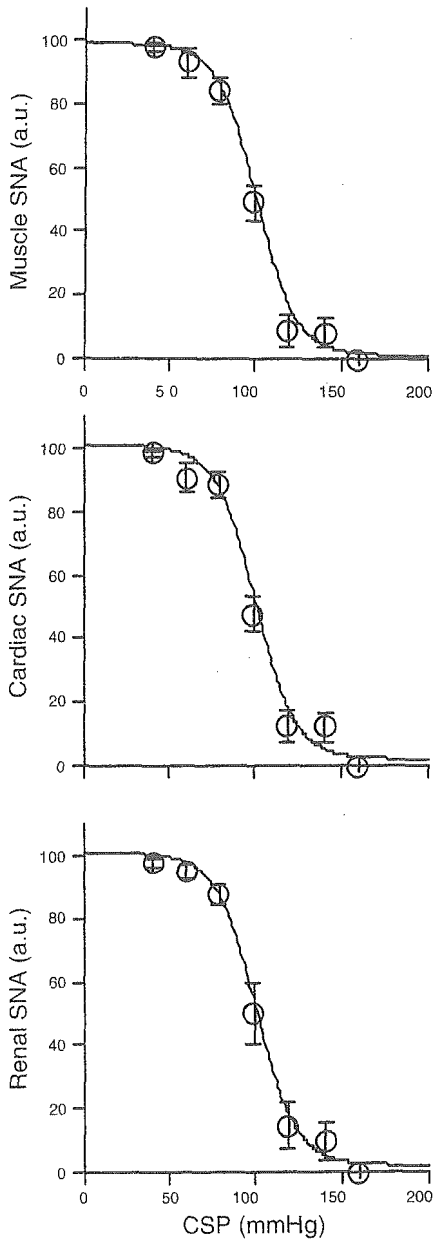

Fig. 2. Static nonlinear, reverse-sigmoidal baroreflex relationship between each SNA (muscle, cardiac, and renal SNA) and CSP from all animals (n = 10) in *protocol 2*. ○, Mean SNA. Error bars denote SD. The static nonlinear characteristics of muscle SNA were similar to those of cardiac and renal SNAs.

The phase of the transfer function from CSP to muscle SNA lagged as frequency increased (Fig. 4*A*), and the frequency-dependent lag was slightly greater than cardiac and renal SNAs. The phase of muscle SNA showed greater lag than that of cardiac SNA from 0.1 to 1 Hz ($P < 0.05$) and than that of renal SNA at 1 Hz ($P < 0.05$) (Table 2).

The coherence of the transfer function from CSP to muscle SNA was over 0.8 between 0.1 and 0.8 Hz, except at ~0.35 Hz (Fig. 4*A*). The coherence of muscle SNA was greater than that of cardiac and renal SNAs at 0.1, 0.8, and 1 Hz ($P < 0.05$) (Table 2).

The step response of muscle SNA to CSP consisted of an initial decrease followed by partial recovery and then steady state (Fig. 4*B*). The initial decrease in muscle SNA was similar

to that in cardiac SNA but greater than that in renal SNA (Fig. 4*B*, Table 2). However, steady-state muscle SNA was similar to that of cardiac and renal SNAs (Fig. 4*B*, Table 2).

DISCUSSION

Despite accumulated knowledge on baroreflex control of muscle SNA, whether the baroreflex control of muscle SNA parallels that of other visceral organs innervated by the sympathetic nervous system, including the kidney and heart, remains unclear. This study has two major new findings. First, the dynamic high-pass characteristic of baroreflex control for muscle SNA, assessed by the increasing slope of transfer gain, is similar to that of cardiac SNA but greater than that of renal SNA. However, the difference is physiologically insignificant, because it may induce detectable differences among SNAs only when AP changes at unphysiologically high rates (see below). Second, the static reverse-sigmoidal relationship between CSP and muscle SNA is almost identical to that of both cardiac and renal SNAs. These findings support our hypothesis to a large extent and indicate that dynamic-linear and static-nonlinear baroreflex control of muscle SNA is similar to that of renal and cardiac SNAs under physiological pressure changes.

The present study quantified the dynamic high-pass characteristics of baroreflex control of muscle SNA by opening the baroreflex feedback loop. In humans, responses of muscle SNA to change in AP is believed to depend on the speed of AP change; more rapid AP change is associated with greater muscle SNA response to AP change. This suggests the presence of high-pass characteristics in the baroreflex control of muscle SNA, and this was actually found in previous human study by sinusoidal modulation of muscle SNA by neck suction at varying frequencies (1). We investigated the transfer function in animals and showed that the transfer gain increased as the frequency of CSP perturbation increased when the increasing slope of transfer gain was 1.84 dB/octave (Table 2). This finding indicates that when CSP changes more rapidly with doubling of the frequency, SNA response increases 1.24 times. In addition, our calculated step response from high-pass transfer function (initial decrease followed by partial recovery, Fig. 4*B*) agrees with the time series of human muscle SNA observed during graded neck pressure or suction (22), supporting the validity of our system identification.

Our data revealed that the dynamic high-pass characteristics of baroreflex control of muscle SNA are similar to those of cardiac SNA but greater than those of renal SNA. In other words, more rapid AP change results in greater muscle SNA in response to pressure change, and this characteristic is similar to cardiac SNA but stronger than renal SNA. Quantitative estimation from the increasing slopes of transfer gain (Table 2) indicates that when the frequency of CSP doubles, the response of cardiac SNA response increases 1.30 times, which is statistically similar to muscle SNA (1.24 times), whereas the response of renal SNA increases 1.13 times and is lower than the muscle and cardiac SNAs. The difference between cardiac and renal SNAs is consistent with previous study (14).

Numerical simulation based on the transfer function estimated by *protocol 2* shows that the differences in dynamic baroreflex control in various organs induce detectable differences among SNAs only when AP changes at very high rates (Fig. 5). According to our previous studies (15), we modeled transfer function of baroreflex control of SNA (see APPENDIX) by setting the parameters of the function to reflect our actual data. The numerical simulation shows that the faster the increasing speed of CSP, the more prominent are the differences among the responses of three SNAs; muscle and cardiac SNAs decrease more markedly than renal SNA (Fig. 5, compare *D*

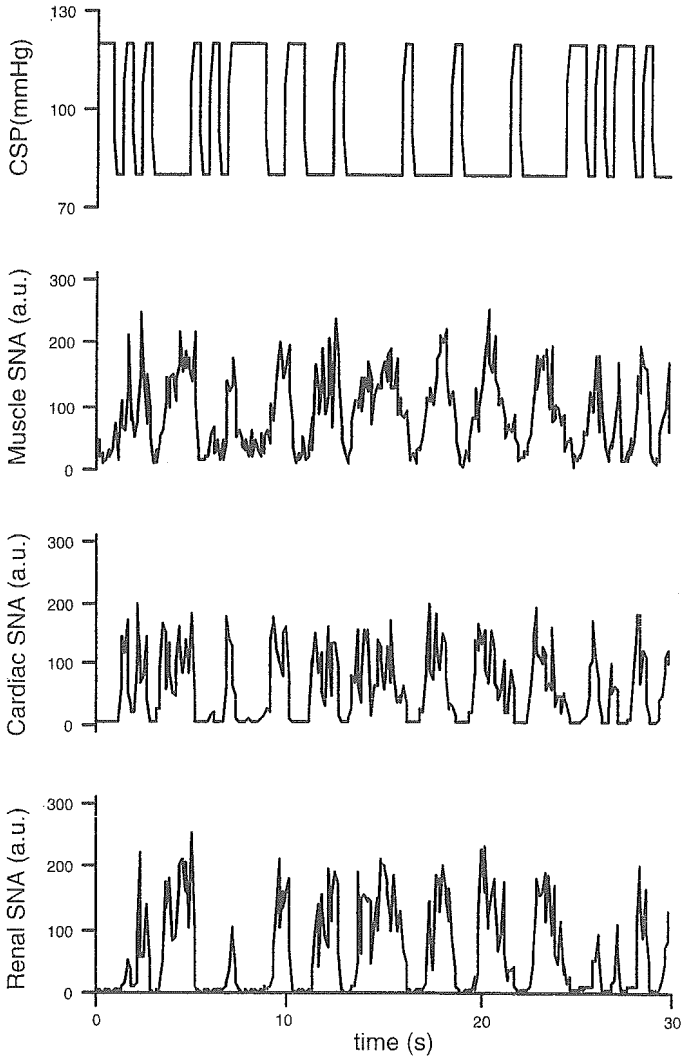

Fig. 3. Representative data of 1 rabbit in *protocol 2*, showing time series of CSP and muscle, cardiac, and renal SNA during CSP perturbation. CSP was changed according to a binary white noise signal with a switching interval of 500 ms.

Table 1. *Four-parameter logistic function fitted to static nonlinear characteristics of baroreflex control of SNA: muscle SNA vs. renal and cardiac SNAs*

	Muscle SNA	Cardiac SNA	Renal SNA
P_1, au	99±1	99±1	98±1
P_2, au/mmHg	0.12±0.02	0.13±0.03	0.12±0.01
P_3, mmHg	102±4	101±4	101±4
P_4, au	0.1±0.3	0.1±0.3	0.1±0.3
G_{max}, au/mmHg	−2.9±0.4	−3.3±0.5	−2.8±0.3

Values are means ± SD (n = 10). See *Eq. 1* in MATERIALS AND METHODS for definition of the 4 parameters (P_1–P_4) of logistic function. All parameters of muscle sympathetic nerve activity (SNA) are similar to those of renal and cardiac SNAs. G_{max}, maximum gain.

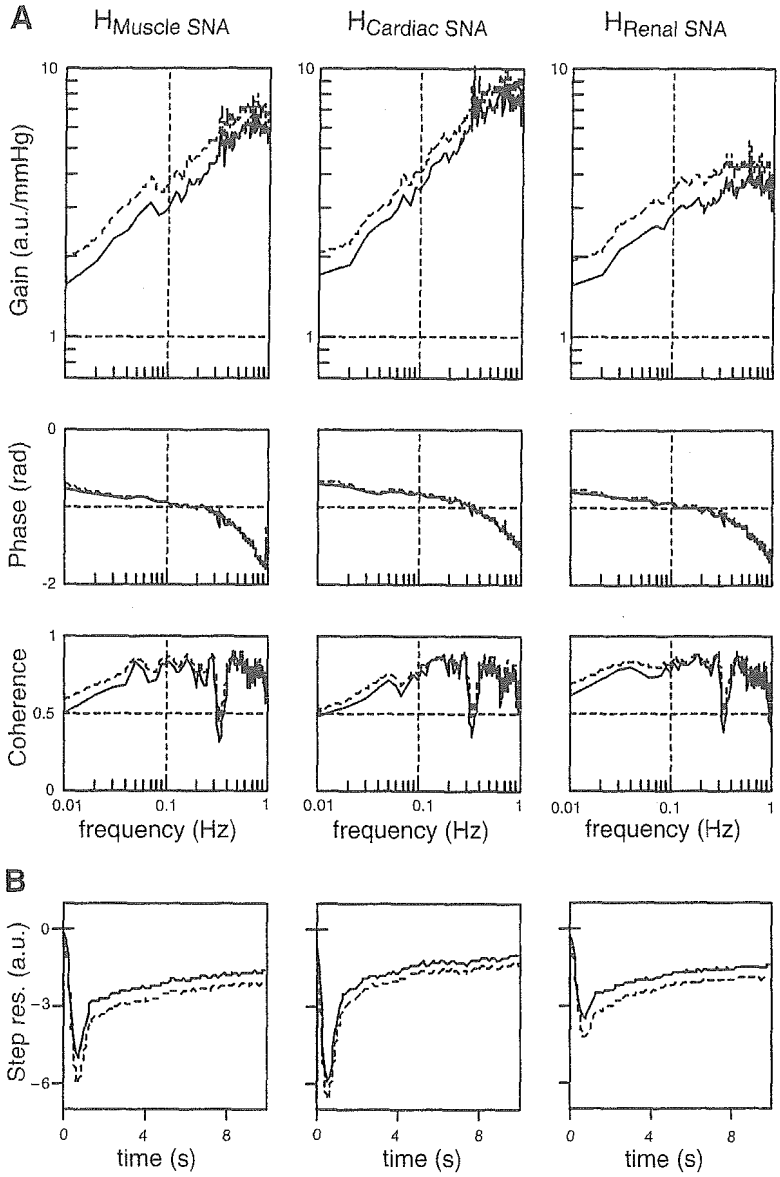

Fig. 4. *A*: transfer function from CSP to renal SNA ($H_{RenalSNA}$), to cardiac SNA ($H_{CardiacSNA}$) and to muscle SNA ($H_{MuscleSNA}$) from all animals (n = 10) in *protocol 2*. Gain plots (*top*), phase plots (*middle*), and coherence function (*bottom*) are shown. Slope of the transfer gain increases more markedly in $H_{MuscleSNA}$ and $H_{CardiacSNA}$ than in $H_{RenalSNA}$. *B*: step responses (Step res) derived from $H_{RenalSNA}$, $H_{CardiacSNA}$, and $H_{MuscleSNA}$. Solid and dashed lines represent mean and mean + SD values, respectively.

and *C* to *B*). However, the organ-dependent differences become detectable only when CSP increases at a high speed of 5 mmHg/s. In clinical situation, AP hardly increases at such high rates even with pharmacological intervention in medical treatment; therefore these SNAs may be similar under physiological pressure changes. Moreover, even if CSP increases at a very high rate, the three SNAs reach similar steady-state activities, reflecting their similar transfer gains at the lowest frequency (Fig. 4*A*, Table 1).

We rigorously investigated the static nonlinear characteristics of baroreflex control of muscle SNA from the relationship between steady-state values of CSP and muscle SNA. Although earlier human studies addressed the reverse-sigmoidal relationship of baroreflex control of muscle SNA using conventional open-loop condition by neck suction and pressure (22) as well as pharmacological (i.e., administration of phenylephrine and nitroprusside) methods (24), these studies failed to determine the relationship in individual subjects. In addition, because these studies analyzed the relationship based on data of dynamically changing SNA in response to changing baroreceptor pressure and not steady-state SNA at constant pressure, the relationship derived should include dynamic linear characteristics of baroreflex control of SNA, and pure static nonlinear characteristics could not be extracted. Given the presence of dynamic characteristics, determining steady-state relationship between SNA and baroreceptor pressure requires keeping the baroreceptor pressure constant until SNA reaches the steady-state level. In the present study (*protocol 1*), we determined the relationship between muscle SNA and CSP at approximately steady state in individual animals.

Our data indicate that static nonlinear characteristics of baroreflex control of muscle SNA are almost identical to those of renal and cardiac SNAs. This finding indicates that steady-state muscle SNA approximates that of renal and cardiac SNA at any baroreceptor pressure. This finding is consistent with the calculated step response of SNA to CSP change (Fig. 4*B*) because muscle SNA reaches the steady-state level similar in magnitude to cardiac and renal SNAs despite differences in the initial rapid decreases at the three sites. This also agrees with the numerical simulation (Fig. 5, *B–D*), which reveals that

Table 2. *Transfer function of baroreflex control of SNA (from CSP to SNA): muscle SNA vs. renal and cardiac SNAs*

	Muscle SNA	Cardiac SNA	Renal SNA
Gain, au/mmHg			
0.01 Hz	1.59±0.39	1.69±0.53	1.56±0.35
0.1 Hz	3.10±0.46	3.48±0.47	2.90±0.43
0.3 Hz	4.36±0.48	5.75±0.41	3.28±0.43*†
0.8 Hz	6.11±0.66	7.71±0.60	3.50±0.44*†
1.0 Hz	5.17±0.72	6.87±0.60	3.02±0.69*†
Phase, rad			
0.01 Hz	−2.34±0.16	−2.29±0.10	−2.51±0.13
0.1 Hz	−2.86±0.04	−2.58±0.04*	−2.92±0.05†
0.3 Hz	−3.48±0.10	−2.98±0.04*	−3.41±0.09†
0.8 Hz	−5.09±0.10	−4.31±0.10*	−4.73±0.10†
1.0 Hz	−5.67±0.10	−4.94±0.09*	−5.30±0.10*†
Coherence			
0.01 Hz	0.52±0.09	0.52±0.03	0.65±0.07
0.1 Hz	0.83±0.03	0.72±0.04*	0.77±0.03*
0.3 Hz	0.83±0.04	0.87±0.02	0.88±0.02
0.8 Hz	0.82±0.03	0.75±0.03*	0.72±0.04*
1.0 Hz	0.61±0.07	0.52±0.08*	0.52±0.08*
Slope, dB/octave (0.01–0.8 Hz)	1.84±0.44	2.28±0.48	1.08±0.18*†
Step response, au			
Initial response	−5.04±0.75	−5.70±0.71	−3.53±0.71*†
Steady-state level	−1.54±0.32	−1.19±0.28	−1.46±0.32

Values are means ± SD (n = 10). CSP, intracarotid sinus pressure. *P < 0.05, muscle SNA vs. renal SNA or cardiac SNA. †P < 0.05, renal SNA vs. cardiac SNA.

these SNAs reach similar steady-state levels even though they respond differently to CSP increase.

The present study may extend earlier studies investigating the relationship between muscle SNA and other SNAs innervating visceral organs (30, 31). These studies reported that microneurographical muscle SNA correlated with norepinephrine spillovers in the heart at rest, handgrip, and mental stress (30), and those in the kidney at rest (31). Although these studies suggested a correlation between muscle SNA and cardiac or renal SNA, they did not assess baroreflex control of SNA. In addition, the spillover measurements may be affected by neurotransmitter kinetics in synapses (release and uptake) and circulating norepinephrine independent of SNA (11), and the method has a low time resolution for assessing the dynamic baroreflex control of SNA. Accordingly, we measured the three SNAs directly and investigated the baroreflex control of each SNA.

Limitations. The present study has several limitations. First, we excluded the efferent effect of vagally mediated arterial baroreflex, which could affect the properties of baroreflex control of SNAs. Second, artificial respiration and surgical procedures used in this study could affect baroreflex. Third, anesthetic agents tend to inhibit efferent SNA and depress the gain of baroreflex control of SNA. Fourth, we used physiological saline preequilibrated with atmospheric air to perfuse the carotid sinuses. Local hypoxia could have occurred and somewhat affected baroreflex control of SNA. Last, although we

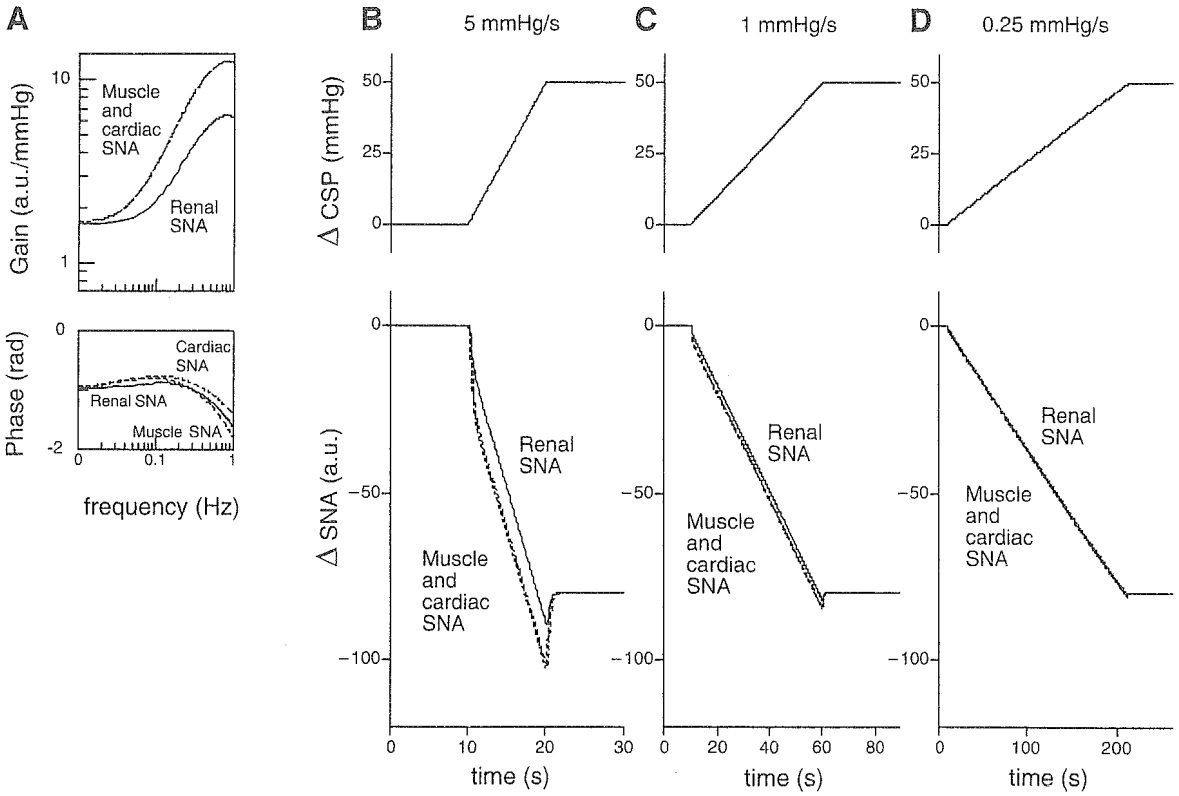

Fig. 5. Simulation of muscle, cardiac, and renal SNA in response to rapid (*B*), moderate (*C*) and slow (*D*) ramp increase in CSP. On the basis of the data from *protocol 2*, the transfer function of baroreflex control of SNA (from CSP input to SNA) is modeled (*A*) as described in APPENDIX. In all panels (except CSP panels), solid, thin dashed, and dashed lines represent the simulation for muscle, cardiac, and renal SNA, respectively. Data of cardiac SNA almost overlap with those of muscle SNA (except Phase panel in *A*). When CSP increases more rapidly (*B*), muscle and cardiac SNAs decrease in response to CSP change more markedly than renal SNA. Of note, time axes are different among panels. The slower the increasing speed of CSP, the smaller the difference among responses of 3 SNAs (*C* and *D*). Despite the difference in dynamic responses, however, all SNAs reach similar steady-state activity levels, regardless of the CSP increasing speed.

held CSP for 60 s at each CSP level in *protocol 1*, some SNAs did not reach steady-state level within 60 s (Fig. 1). Therefore, the duration may be short to obtain steady-state SNA in all cases. However, because holding CSP for longer periods can induce SNA changes originating from factors other than CSP change itself, it is difficult to know precisely when SNA reaches steady-state level. Future study is needed to examine pure static baroreflex characteristics.

In summary, dynamic high-pass characteristics of baroreflex control of muscle SNA, assessed by the increasing slope of transfer gain, showed that more rapid change of arterial pressure resulted in greater response of muscle SNA to pressure change and that these characteristics were similar to cardiac SNA but greater than renal SNA. However, the numerical simulation based on the transfer function shows that the differences in dynamic baroreflex control at various organs result in detectable difference among SNAs only when AP changes at unphysiologically high rates (i.e., 5 mmHg/s). In addition, static reverse-sigmoid characteristics of baroreflex control of muscle SNA are almost identical with those of renal or cardiac SNAs. We conclude that dynamic-linear and static-nonlinear baroreflex control of muscle SNA is similar to that of renal and cardiac SNAs, with the exception of a mildly reduced dynamic-linear response of renal SNA to rapid pressure change outside the physiological range.

APPENDIX

In rabbits, the transfer function of the baroreflex neural arc (baroreceptor pressure to SNA) approximates derivative characteristics in the frequency range below 0.8 Hz and high-cut characteristics of frequencies above 0.8 Hz (15). Therefore, according to our previous study (15), we model the neural arc transfer function (H_N) using *Eq. A1* as follows

$$H_N(f) = -K_N \frac{1 + \frac{f}{f_{c1}} j}{\left(1 + \frac{f}{f_{c2}}\right)^2} \exp(-2\pi f j L) \qquad (A1)$$

where f and j represent the frequency (in Hz) and imaginary units, respectively; K_N is static gain (in au/mmHg); f_{c1} and f_{c2} ($f_{c1} < f_{c2}$) are corner frequencies (in Hz) for derivative and high-cut characteristics, respectively; and L is a pure delay (in s) that would represent the sum of delays in the synaptic transmission at the baroreflex central pathways and the sympathetic ganglion. The dynamic gain increases in the frequency range from f_{c1} to f_{c2} and decreases above f_{c2}. On the basis of the measured results from *protocol 1*, we set K_N at 1.6 and f_{c2} at 0.8 similarly in all of muscle, cardiac, and renal SNAs in simulations shown in Fig. 5. In addition, we set f_{c1} at 0.05, 0.05, and 0.1, respectively, in muscle, cardiac and renal SNA. We also set L at 0.3, 0.1 and 0.2, respectively, corresponding to the distance of neural pathway from carotid sinus region to the tibial, cardiac, and renal sympathetic nerve.

GRANTS

This study is a part of the "Ground-Based Research Announcement for Space Utilization" project promoted by Japan Space Forum. This study was also supported by Industrial Technology Research Grant Program 03A47075 from New Energy and Industrial Technology Development Organization (NEDO) of Japan.

REFERENCES

1. **Bernardi L, Hayoz D, Wenzel R, Passino C, Calciati A, Weber R, and Noll G.** Synchronous and baroceptor-sensitive oscillations in skin microcirculation: evidence for central autonomic control. *Am J Physiol Heart Circ Physiol* 273: H1867–H1878, 1997.
2. **Cooke WH, Hoag JB, Crossman AA, Kuusela TA, Tahvanainen KU, and Eckberg DL.** Human responses to upright tilt: a window on central autonomic integration. *J Physiol* 517: 617–628, 1999.
3. **Eckberg DL and Sleight P.** *Human Baroreflexes in Health and Disease.* New York: Oxford Univ. Press, 1992.
4. **Fadel PJ, Ogoh S, Watenpaugh DE, Wasmund W, Olivencia-Yurvati A, Smith ML, and Raven PB.** Carotid baroreflex regulation of sympathetic nerve activity during dynamic exercise in humans. *Am J Physiol Heart Circ Physiol* 280: H1383–H1390, 2001.
5. **Furlan R, Diedrich A, Rimoldi A, Palazzolo L, Porta C, Diedrich L, Harris PA, Sleight P, Biagioni I, Robertson D, and Bernardi L.** Effects of unilateral and bilateral carotid baroreflex stimulation on cardiac and neural sympathetic discharge oscillatory patterns. *Circulation* 108: 717–723, 2003.
6. **Graham LN, Smith PA, Stoker JB, Mackintosh AF, and Mary DA.** Time course of sympathetic neural hyperactivity after uncomplicated acute myocardial infarction. *Circulation* 106: 793–797, 2002.
7. **Grassi G, Cattaneo BM, Seravalle G, Lanfranchi A, and Mancia G.** Baroreflex control of sympathetic nerve activity in essential and secondary hypertension. *Hypertension* 31: 68–72, 1998.
8. **Grassi G, Seravalle G, Cattaneo BM, Lanfranchi A, Vailati S, Giannattasio C, Del Bo A, Sala C, Bolla GB, and Pozzi M.** Sympathetic activation and loss of reflex sympathetic control in mild congestive heart failure. *Circulation* 92: 3206–3211, 1995.
9. **Halliwill JR, Morgan BJ, and Charkoudian N.** Peripheral chemoreflex and baroreflex interactions in cardiovascular regulation in humans. *J Physiol* 552: 295–302, 2003.
10. **Hansen J and Sander M.** Sympathetic neural overactivity in healthy humans after prolonged exposure to hypobaric hypoxia. *J Physiol* 546: 921–929, 2003.
11. **Jennings GL.** Noradrenaline spillover and microneurography measurements in patients with primary hypertension. *J Hypertens Suppl* 16: S35–S38, 1998.
12. **Kamiya A, Michikami D, Fu Q, Niimi Y, Iwase S, Mano T, and Suzumura A.** Static handgrip exercise modifies arterial baroreflex control of vascular sympathetic outflow in humans. *Am J Physiol Regul Integr Comp Physiol* 281: R1134–R1139, 2001.
13. **Kamiya A, Michikami D, Hayano J, and Sunagawa K.** Heat stress modifies human baroreflex function independently of heat-induced hypovolemia. *Jpn J Physiol* 53: 215–222, 2003.
14. **Kawada T, Shishido T, Inagaki M, Tatewaki T, Zheng C, Yanagiya Y, Sugimachi M, and Sunagawa K.** Differential dynamic baroreflex regulation of cardiac and renal sympathetic nerve activities. *Am J Physiol Heart Circ Physiol* 280: H1581–H1590, 2001.
15. **Kawada T, Zheng C, Yanagiya Y, Uemura K, Miyamoto T, Inagaki M, Shishido T, Sugimachi M, and Sunagawa K.** High-cut characteristics of the baroreflex neural arc preserve baroreflex gain against pulsatile pressure. *Am J Physiol Heart Circ Physiol* 282: H1149–H1156, 2002.
16. **Mano T.** Microneurography as a tool to investigate sympathetic nerve responses to environmental stress. *Aviakosmicheskaia Ekologicheskaia Meditsina* 31: 8–14, 1997.
17. **Markel TA, Daley JC III, Hogeman CS, Herr MD, Khan MH, Gray KS, Kunselman AR, and Sinoway LI.** Aging and the exercise pressor reflex in humans. *Circulation* 107: 675–678, 2003.
18. **Mitchell JH and Victor RG.** Neural control of the cardiovascular system: insights from muscle sympathetic nerve recordings in humans. *Med Sci Sports Exerc* 28: S60–S69, 1996.
19. **Mosqueda-Garcia R, Furlan R, Tank J, and Fernandez-Violante R.** The elusive pathophysiology of neurally mediated syncope. *Circulation* 102: 2898–2906, 2000.
20. **Nakamura T, Kawahara K, Kusunoki M, and Feng Z.** Microneurography in anesthetized rats for the measurement of sympathetic nerve activity in the sciatic nerve. *J Neurosci Methods* 131: 35–39, 2003.
21. **Narkiewicz K, Pesek CA, Kato M, Phillips BG, Davison DE, and Somers VK.** Baroreflex control of sympathetic nerve activity and heart rate in obstructive sleep apnea. *Hypertension* 32: 1039–1043, 1998.
22. **Rea RF and Eckberg DL.** Carotid baroreceptor-muscle sympathetic relation in humans. *Am J Physiol Regul Integr Comp Physiol* 253: R929–R934, 1987.

23. **Rowell LB.** *Human Cardiovascular Control.* New York: Oxford Univ. Press, 1993.
24. **Rudas L, Crossman AA, Morillo CA, Halliwill JR, Tahvanainen KU, Kuusela TA, and Eckberg DL.** Human sympathetic and vagal baroreflex responses to sequential nitroprusside and phenylephrine. *Am J Physiol Heart Circ Physiol* 276: H1691–H1698, 1999.
25. **Scherrer U, Pryor SL, Bertocci LA, and Victor RG.** Arterial baroreflex buffering of sympathetic activation during exercise-induced elevations in arterial pressure. *J Clin Invest* 86: 1855–1861, 1990.
26. **Sundlof G and Wallin BG.** Human muscle nerve sympathetic activity at rest. Relationship to blood pressure and age. *J Physiol* 274: 621–637, 1978.
27. **Tanaka H, Davy KP, and Seals DR.** Cardiopulmonary baroreflex inhibition of sympathetic nerve activity is preserved with age in healthy humans. *J Physiol* 515: 249–254, 1999.
28. **Van De Borne P, Mezzetti S, Montano N, Narkiewicz K, Degaute JP, and Somers VK.** Hyperventilation alters arterial baroreflex control of heart rate and muscle sympathetic nerve activity. *Am J Physiol Heart Circ Physiol* 279: H536–H541, 2000.
29. **Wallin BG and Eckberg DL.** Sympathetic transients caused by abrupt alterations of carotid baroreceptor activity in humans. *Am J Physiol Heart Circ Physiol* 242: H185–H190, 1982.
30. **Wallin BG, Esler M, Dorward P, Eisenhofer G, Ferrier C, Westerman R, and Jennings G.** Simultaneous measurements of cardiac noradrenaline spillover and sympathetic outflow to skeletal muscle in humans. *J Physiol* 453: 45–58, 1992.
31. **Wallin BG, Thompson JM, Jennings GL, and Esler MD.** Renal noradrenaline spillover correlates with muscle sympathetic activity in humans. *J Physiol* 491: 881–887, 1996.

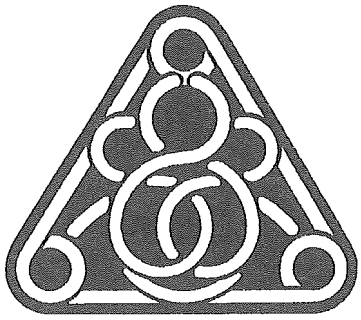

Am J Physiol Heart Circ Physiol 289: H1758–H1769, 2005.
First published June 2, 2005; doi:10.1152/ajpheart.01027.2004.

Low-frequency oscillation of sympathetic nerve activity decreases during development of tilt-induced syncope preceding sympathetic withdrawal and bradycardia

Atsunori Kamiya,[1,3] Junichiro Hayano,[2] Toru Kawada,[1] Daisaku Michikami,[1,3] Kenta Yamamoto,[1] Hideto Ariumi,[1] Syuji Shimizu,[1] Kazunori Uemura,[1] Tadayoshi Miyamoto,[1] Takeshi Aiba,[1] Kenji Sunagawa,[4] and Masaru Sugimachi[1]

[1]*Department of Cardiovascular Dynamics, National Cardiovascular Center Research Institute, Osaka;* [2]*Core Laboratory, Nagoya City University Graduate School of Medical Sciences, and* [3]*Department of Autonomic Neuroscience, Research Institute of Environmental Medicine, Nagoya University, Nagoya; and* [4]*Department of Cardiovascular Medicine, Kyusyu University Graduate School of Medical Sciences, Fukuoka, Japan*

Submitted 6 October 2004; accepted in final form 31 May 2005

Kamiya, Atsunori, Junichiro Hayano, Toru Kawada, Daisaku Michikami, Kenta Yamamoto, Hideto Ariumi, Syuji Shimizu, Kazunori Uemura, Tadayoshi Miyamoto, Takeshi Aiba, Kenji Sunagawa, and Masaru Sugimachi. Low-frequency oscillation of sympathetic nerve activity decreases during development of tilt-induced syncope preceding sympathetic withdrawal and bradycardia. *Am J Physiol Heart Circ Physiol* 289: H1758–H1769, 2005. First published June 2, 2005; doi:10.1152/ajpheart.01027.2004.—Sympathetic activation during orthostatic stress is accompanied by a marked increase in low-frequency (LF, ~0.1-Hz) oscillation of sympathetic nerve activity (SNA) when arterial pressure (AP) is well maintained. However, LF oscillation of SNA during development of orthostatic neurally mediated syncope remains unknown. Ten healthy subjects who developed head-up tilt (HUT)-induced syncope and 10 age-matched nonsyncopal controls were studied. Nonstationary time-dependent changes in calf muscle SNA (MSNA, microneurography), R-R interval, and AP (finger photoplethysmography) variability during a 15-min 60° HUT test were assessed using complex demodulation. In both groups, HUT during the first 5 min increased heart rate, magnitude of MSNA, LF and respiratory high-frequency (HF) amplitudes of MSNA variability, and LF and HF amplitudes of AP variability but decreased HF amplitude of R-R interval variability (index of cardiac vagal nerve activity). In the nonsyncopal group, these changes were sustained throughout HUT. In the syncopal group, systolic AP decreased from 100 to 60 s before onset of syncope; LF amplitude of MSNA variability decreased, whereas magnitude of MSNA and LF amplitude of AP variability remained elevated. From 60 s before onset of syncope, MSNA and heart rate decreased, index of cardiac vagal nerve activity increased, and AP further decreased to the level at syncope. LF oscillation of MSNA variability decreased during development of orthostatic neurally mediated syncope, preceding sympathetic withdrawal, bradycardia, and severe hypotension, to the level at syncope.

autonomic nervous system; baroreflex; blood pressure; heart rate variability; hemodynamics

HUMANS HAVE BEEN SUBJECTED to ceaseless orthostatic stresses since they first evolved and assume an orthostatic posture for most of their lives. During standing, gravitational fluid shift toward the lower part of body (i.e., abdominal vascular bed and lower limbs) would cause severe orthostatic hypotension if it were not countered by compensatory mechanisms (23). Orthostatic sympathetic activation has a crucial role in preventing orthostatic hypotension and maintaining arterial blood pressure (AP) (23). Recent studies have reported that orthostatic sympathetic activation is accompanied by an increase in low-frequency (LF, ~0.1-Hz) oscillation of sympathetic nerve activity (SNA) (1, 5). Tilt maneuvers of 75° and 80° greatly increase the LF oscillatory patterns of muscle SNA (MSNA), which mirrored similar changes in LF oscillation of AP (1, 5). However, LF oscillation of SNA has been investigated only in the steady-state orthostatic condition, when AP remains well maintained. It remains unclear whether LF oscillation of SNA changes during development of orthostatic neurally mediated syncope. Syncope is a common and potentially dangerous clinical syndrome (18). Under this condition, a major cause of hypotension is paradoxical withdrawal of sympathetic outflow to resistance vessels, because MSNA is greatly inhibited during hypotension (16–18), in addition to cardiac vagal excitation. Inasmuch as sympathetic activation is known to be accompanied by an increase in LF oscillation of SNA (1, 5, 15, 20, 24), it is possible that the increase in LF oscillation of SNA during orthostatic stress is not sustained during sympathetic withdrawal in the course of development of orthostatic neurally mediated syncope. Therefore, we hypothesized that LF oscillation of SNA decreases during development of orthostatic neurally mediated syncope. Because detailed characteristics, including LF oscillations of SNA during development of syncope, have not been studied in detail, we examine this phenomenon and attempt to explain the mechanism involved on the basis of current theories.

To test the hypothesis, we analyzed MSNA (by microneurography) and AP in 10 healthy male volunteers who manifested orthostatic neurally mediated syncope during the head-up tilt (HUT) test. Because sympathetic and cardiovascular changes during development of syncope are sudden and time dependent, traditional spectral methods, including autoregressive and fast Fourier transform power spectral analyses, cannot be used to assess these parameters. We therefore used the complex demodulation technique (8, 9, 13) to investigate dynamic changes in amplitudes of LF and respiratory high-

Address for reprint requests and other correspondence: A. Kamiya, Dept. of Cardiovascular Dynamics, National Cardiovascular Center Research Institute, 5-7-1 Hujishirodai, Suita, Osaka 565-8565, Japan (E-mail: kamiya@ri.ncvc.go.jp).

The costs of publication of this article were defrayed in part by the payment of page charges. The article must therefore be hereby marked "*advertisement*" in accordance with 18 U.S.C. Section 1734 solely to indicate this fact.

frequency (HF, ~0.25-Hz) oscillations of MSNA before and during tilt-induced orthostatic neurally mediated syncope.

METHODS

Subjects. Twenty healthy male volunteers [24 ± 4 (SE) yr old, 171 ± 5 cm, and 66 ± 5 kg body wt] underwent a passive 60° HUT test as described below. Ten of the subjects who developed orthostatic neurally mediated syncope or presyncope (syncopal group) were matched to 10 who remained asymptomatic during the procedure. Subjects with and without syncope were matched by age. The subjects were recruited from the local community through advertising on a notice board. They were carefully screened, with a medical history, physical examination, complete blood count, blood chemistry analyses, electrocardiogram, and psychological testing. Potential subjects with cardiovascular or other disease were excluded, as well as those who smoked tobacco products, drank alcohol, took medications other than oral contraceptives, or were obese (body mass index >30 kg/m^2). None of the subjects had experienced spontaneous syncope within the past 5 yr. All subjects had a sedentary lifestyle, and none were athletes. All subjects gave informed consent to participate in the study, which was approved by the Committee of Human Research of Research Institute of Environmental Medicine at Nagoya University.

Measurements. AP was measured continuously using a finger photoplethysmograph (Finapres, model 2300, Ohmeda, Englewood, CO). Systolic, diastolic, and pulse pressures were measured from the continuous pressure wave. Mean pressure was calculated by averaging pressure within a pulse wave. Finger pressure was confirmed to match intermittent (every minute) brachial AP measured by an automated sphygmomanometer (model BP203MII, Nippon Colin, Komaki, Japan). Electrocardiogram (chest lead II) and thermistor respirogram were also recorded continuously.

MSNA was measured as reported previously by our laboratory (14). Briefly, a tungsten microelectrode (model 26-05-1, Frederick Haer, Bowdoinham, ME) was inserted percutaneously into the muscle nerve fascicles of the tibial nerve at the right popliteal fossa without anesthesia. Nerve signals were fed into a preamplifier (Kohno Instruments, Nagoya, Japan) with two active band-pass filters set between 500 and 5,000 Hz and monitored with a loudspeaker. MSNA was identified according to the following discharge characteristics: *1*) pulse-synchronous and spontaneous efferent discharges, *2*) afferent activity evoked by tapping calf muscles, but not in response to a gentle skin touch, and *3*) enhancement during phase II of the Valsalva maneuver.

Protocols. Subjects were instructed to refrain from eating for 3 h before the experiments, which were conducted in an air-conditioned (26°C) room. Each subject was required to remain supine on a tilt bed set at 0° horizontally. After the microneurographic MSNA signal was detected, the subject remained at 0° supine and at rest for ≥20 min; then baseline MSNA, blood pressure, electrocardiogram, and respiration were recorded for 6 min. Thereafter, the tilt table was inclined to 60° in a passive manner and fixed for 15 min. The HUT was terminated and the table was returned to the 0° horizontal position when any of the following findings was observed: development of presyncope symptoms such as nausea, sweating, yawning, gray out, and dizziness and progressive reduction in systolic blood pressure to <80 mmHg. All variables were continuously monitored.

Data analysis. The full-wave-rectified MSNA signal was fed through a resistance-capacitance low-pass filter at a time constant of 0.1 s to obtain the mean voltage neurogram, which was resampled at 200 Hz, together with other cardiovascular variables. MSNA bursts were identified, and their areas were calculated using a custom-built (by our laboratory) computer program. MSNA was expressed as the rate of integrated activity per minute (burst rate) and total activity by integrating individual burst area per minute (total MSNA). Because burst area and, hence, total MSNA were dependent on electrode position, they were expressed as arbitrary units (AU) normalized by the individual baseline value at 0° supine rest (average of total MSNA per minute during 6 min of 0° supine rest was given an arbitrary value of 100 AU). The area of each burst during HUT was normalized to this value.

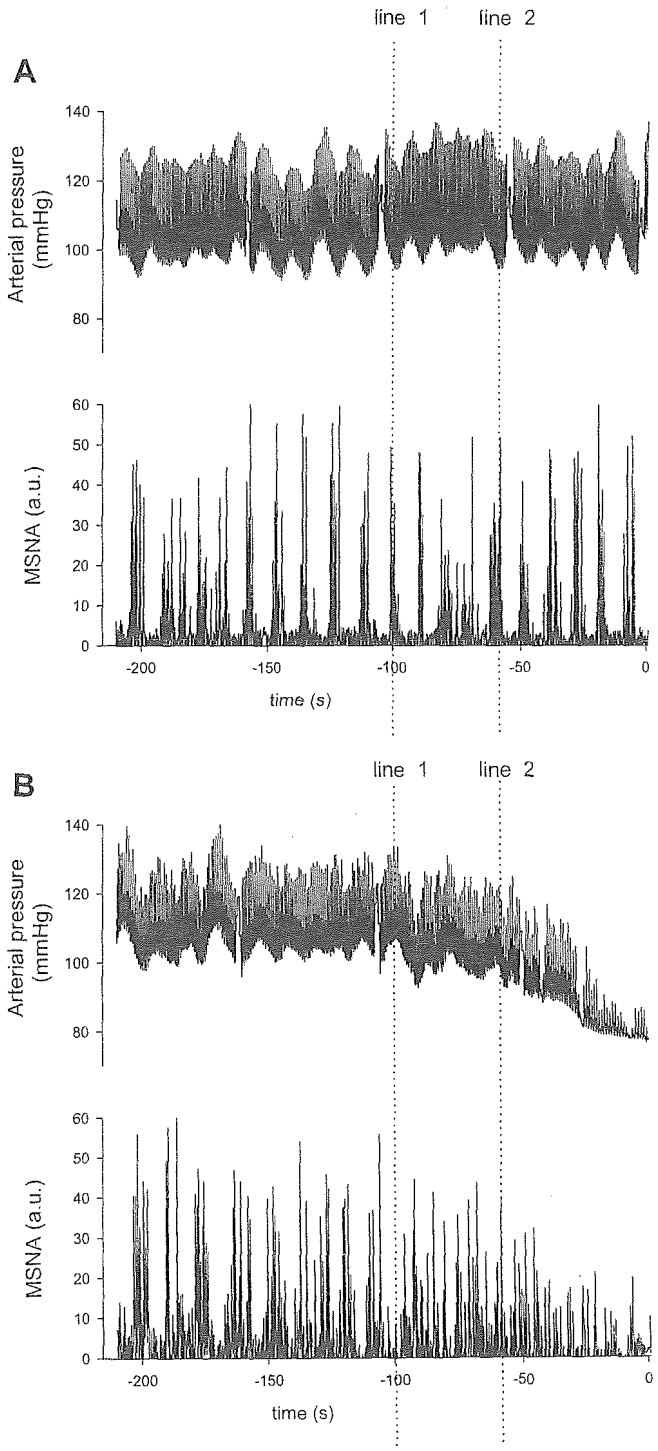

Fig. 1. Representative recordings of arterial pressure (AP) and muscle sympathetic nerve activity (MSNA, integrated signals) over 210 s before completion of head-up tilt (HUT) test in a nonsyncopal subject (*A*) and onset of syncope evoked by 60° HUT in a syncopal subject (*B*). *Time 0*, completion of HUT test (*A*) or onset of syncope when systolic AP decreases below 80 mmHg (*B*). *Line 1* and *line 2*, 100 and 60 s, respectively, before onset of syncope in HUT test.